Article

Bacteria conjugate ubiquitin-like proteins to interfere with phage assembly

https://doi.org/10.1038/s41586-024-07616-5

Received: 24 August 2023

Accepted: 28 May 2024

Published online: 17 July 2024

Check for updates

Jens Hör[1,3], Sharon G. Wolf[2] & Rotem Sorek[1]✉

Several immune pathways in humans conjugate ubiquitin-like proteins to virus and host molecules as a means of antiviral defence[1–5]. Here we studied an antiphage defence system in bacteria, comprising a ubiquitin-like protein, ubiquitin-conjugating enzymes E1 and E2, and a deubiquitinase. We show that during phage infection, this system specifically conjugates the ubiquitin-like protein to the phage central tail fibre, a protein at the tip of the tail that is essential for tail assembly as well as for recognition of the target host receptor. Following infection, cells encoding this defence system release a mixture of partially assembled, tailless phage particles and fully assembled phages in which the central tail fibre is obstructed by the covalently attached ubiquitin-like protein. These phages show severely impaired infectivity, explaining how the defence system protects the bacterial population from the spread of phage infection. Our findings demonstrate that conjugation of ubiquitin-like proteins is an antiviral strategy conserved across the tree of life.

Ubiquitin is a conserved eukaryotic protein that can be covalently attached to target proteins as part of the protein degradation pathway[6]. Covalent attachment of ubiquitin necessitates a cascade of enzymatic reactions carried out by three classes of proteins called E1, E2 and E3 (ref. 6). The E1 enzyme first adenylates a conserved C-terminal glycine residue in the ubiquitin protein and then covalently attaches the adenylated ubiquitin to a conserved cysteine in the E1 active site[6]. The ubiquitin is then transferred to a cysteine residue in the E2 enzyme, which further transfers it to the target protein, usually by means of a mediator E3 protein[6]. Ubiquitination can be reversed by deubiquitinases (DUBs), which are peptidases capable of removing ubiquitin from target molecules[7].

Although ubiquitination of proteins is central to the protein degradation pathway in humans[8], conjugation of ubiquitin and ubiquitin-like proteins (Ubls) was also shown to be important in pathways of innate immunity[1,2]. For example, interferon-stimulated gene 15 (ISG15) is a Ubl composed of two fused ubiquitin-like domains, which is involved in protecting human cells against a variety of viruses such as influenza A and HIV-1 (ref. 5). ISG15 is one of the most highly upregulated genes following virus-induced type I interferon stimulation[9], and its specific E1, E2 and E3 enzymes are also interferon induced[10]. It was shown that during virus infection, ISG15 is intracellularly conjugated to several cellular and viral protein targets, impairing viral propagation through a mechanism that is still unclear[3–5].

Like eukaryotes, bacteria can also be infected by viruses (phages), against which bacteria have evolved a plethora of immune defence strategies[11,12]. A recent screen for antiphage defence systems in bacteria revealed a four-gene operon encoding a Ubl protein, a protein with a predicted E1 domain, a protein with a predicted E2 domain and a protein with a predicted DUB domain[13] (Fig. 1a). Similar to ISG15, the Ubl in this bacterial system is composed of two fused ubiquitin domains, and the operon was accordingly denoted BilABCD (standing for bacterial ISG15-like system). The Bil defence system was previously shown to protect bacteria against many phages, but the mechanism of defence remained unknown[13].

In this study, we show that the Bil system covalently conjugates its Ubl protein to the phage central tail fibre (CTF), an essential structural component of the phage tail tip that is crucial for both tail assembly[14] and host recognition[15]. Conjugation of the Ubl to the CTF inhibits tail assembly, leading to the production of non-infective, tailless phages. In some cases, phages manage to assemble fully tailed particles, but in these particles the Ubl is covalently attached to the CTF at the tip of the tail, impairing infectivity probably by inhibiting host recognition. Thus, the Bil system prevents the spread of phages to neighbouring cells after the initially infected bacterium is lysed, and protects the bacterial population as a whole. Our study reveals a new mechanism used by bacteria to defend against phage predation and sheds light on the mechanism of Ubl-mediated immunity.

Ubl conjugation by the Bil system

We set out to study the BilABCD system from *Collimonas* sp. OK412, a four-gene operon encoding the Ubl protein BilA, the E2 domain protein BilB, the DUB BilC and the E1 domain protein BilD (Fig. 1a). When heterologously expressed in *Escherichia coli*, this system was previously shown to protect against propagation of many coliphages[13]. Structural analysis using AlphaFold2 (ref. 16) revealed that the bacterial Ubl protein contains two fused ubiquitin-like domains, both of which are structurally highly similar to human ubiquitin (Fig. 1b). The last amino acid at the C terminus of the bacterial Ubl is glycine, which is fully conserved among all homologues of the BilA Ubl (Fig. 1c and Extended Data Fig. 1a). As the C-terminal residue of Ubls is an obligatory glycine whose carboxyl group is the site of conjugation to targets[6], conservation of glycine at the C terminus of the bacterial Ubl suggests

[1]Department of Molecular Genetics, Weizmann Institute of Science, Rehovot, Israel. [2]Department of Chemical Research Support, Weizmann Institute of Science, Rehovot, Israel. [3]Present address: Helmholtz Institute for RNA-based Infection Research (HIRI), Helmholtz Centre for Infection Research (HZI), Würzburg, Germany. ✉e-mail: rotem.sorek@weizmann.ac.il

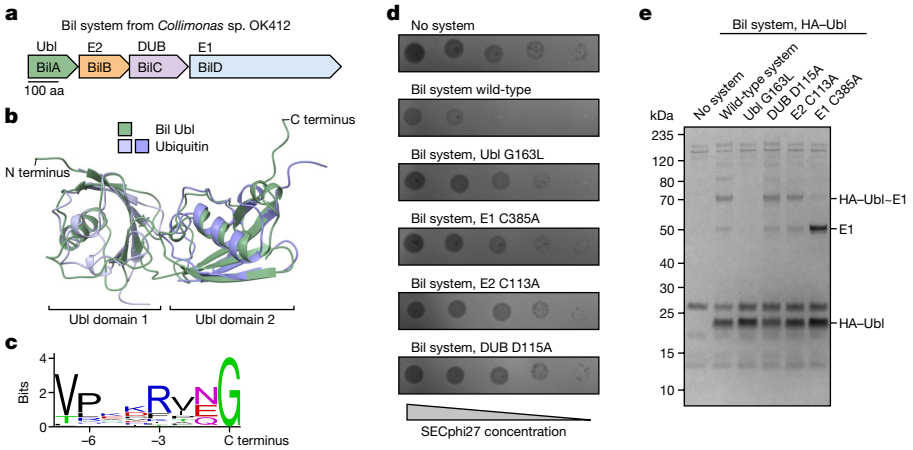


Fig. 1 | Features of ubiquitin-like conjugation in the Bil antiphage defence system. a, Operon structure of the Bil system from *Collimonas* sp. OK412. aa, amino acids. **b**, Structure of the BilA Ubl protein, predicted by AlphaFold2 (ref. 16). The N- and C-terminal Ubl domains were each aligned separately to human ubiquitin (Protein Data Bank 1UBQ, ref. 43) with r.m.s.d. values of 1.62 and 1.77 Å, respectively. **c**, C-terminal sequence conservation among 77 homologues (Supplementary Table 6) of the Ubl protein of the Bil system. **d**, Plaque assays showing the defence phenotype of the wild-type and mutant Bil systems against phage SECphi27. Data are representative of three biological experiments. PFU quantification is presented in Extended Data Fig. 1b. **e**, Immunoprecipitation of HA-tagged Ubl protein from wild-type and mutant Bil system-expressing bacteria, analysed using SDS–PAGE followed by Coomassie staining. Verification of the HA–Ubl-E1 and E1 bands through mass spectrometry is presented in Extended Data Fig. 1e,g. A representative image of three biological replicates is shown.

that, similar to other known Ubl systems, conjugation to the target occurs through this residue. Indeed, a single amino acid substitution at this position (G163L) was sufficient to abolish phage defence by the Bil system (Fig. 1d and Extended Data Fig. 1b).

The first step in any Ubl conjugation cascade involves adenylation of the Ubl, followed by formation of a covalent thioester bond between the E1 enzyme and the Ubl (ref. 17) (Extended Data Fig. 1c). To examine whether a covalent Ubl-E1 complex is formed by the bacterial system, we tagged the E1 protein in the system and performed western blot analysis on total protein extracted from cells expressing the Bil system (Extended Data Fig. 1d). This analysis revealed two bands for the E1 protein, one of the expected size of free tagged E1 (roughly 53 kDa) and one that was roughly 20 kDa larger than the free E1, suggesting linkage to a single Ubl (roughly 18 kDa). The addition of dithiothreitol (DTT), which reduces thioester bonds[18], resulted in the disappearance of this extra band, further supporting the hypothesis that this band represents a Ubl-E1 covalent complex (Extended Data Fig. 1d).

Immunoprecipitation of an N-terminally HA-tagged Ubl further confirmed that a Ubl-E1 complex is formed in cells expressing the Bil system, which was verified by mass spectrometry of the roughly 70 kDa band (Fig. 1e and Extended Data Fig. 1e). The covalent Ubl-E1 complex was lost when the conserved cysteine at the active site of the E1 protein (C385) was substituted to alanine (Fig. 1e). The C385A substitution also abolished the ability of the Bil system to protect against phages[13], indicating that conjugation of the Ubl by the E1 enzyme is essential for the defensive function (Fig. 1d and Extended Data Fig. 1b). Structural analysis with AlphaFold-Multimer[19] predicted a high-confidence interaction between the two proteins that involves the penetration of the Ubl C terminus into the E1 adenylation site (Extended Data Fig. 1f). This places the C-terminal glycine of the Ubl at the nucleotide-binding loop of the E1, thus providing a structural explanation for the mechanism of the first step of the Ubl-E1 conjugation (Extended Data Fig. 1c). The structure further predicts a substantial non-covalent interaction interface between the E1 and the Ubl, explaining why the Ubl can pull down the C385A E1 protein even in the absence of covalent interactions (Fig. 1e and Extended Data Fig. 1f,g).

The second step in the Ubl conjugation cascade is the transfer of the Ubl from the cysteine of the E1 to a cysteine of the E2 (ref. 17) (Extended Data Fig. 1c). We were unable to detect a thioester-linked Ubl-E2 complex, suggesting that this complex might be transient (Extended Data Fig. 1h). However, amino acid substitution in the predicted active site of the E2 (C113A) abolished defence against phages, as previously shown[13], further supporting the hypothesis that Ubl conjugation is central for the defensive function of the Bil system (Fig. 1d and Extended Data Fig. 1b). In the final step, the Ubl is conjugated to a lysine residue of the target protein by the E2, as was recently suggested by a structural study of a Bil system homologue[20] (Extended Data Fig. 1c). Disruption of the predicted active site of the DUB (D115A) also abolished phage defence of the Bil system, suggesting that its deubiquitination enzymatic activity is essential for the function of the system (Fig. 1d and Extended Data Fig. 1b).

To assess the influence of the Bil system expression levels on antiphage defence, we expressed the system under the control of a tetracycline-inducible promoter, which allows for tight transcriptional control[21]. We found that defence could be observed at inducer concentrations as low as 25 ng ml^{-1} (roughly 54 nM) (Extended Data Fig. 2a). Whole-transcriptome RNA sequencing (RNA-seq) analysis revealed that at this concentration of inducer, Bil system genes show expression levels similar to chromosomally encoded defence systems that are naturally present in our model *E. coli* host, including type I and type IV RM systems, TA systems and abortive infection genes (Extended Data Fig. 2b). Furthermore, RNA-seq of *Caulobacter* sp. Root343, a plant root-associated bacterium that naturally encodes a functional Bil system[13], revealed that the Bil system is constitutively expressed in amounts comparable to other defence systems encoded in the *Caulobacter* genome (Extended Data Fig. 2c). These results indicate that the Bil system defends against phages when expressed at levels mimicking physiological expression levels.

The Bil system disrupts phage assembly

We next conducted liquid culture infection assays with SECphi27, a phage from the *Drexlerviridae* family against which the Bil system provides substantial protection in plaque assay experiments (Fig. 1d and Extended Data Fig. 1b). Cells expressing the Bil system survived phage infection in liquid culture when phages were supplied at low multiplicity of infection (MOI), but when infected at high MOI the culture completely collapsed (Fig. 2a). These culture dynamics are similar to

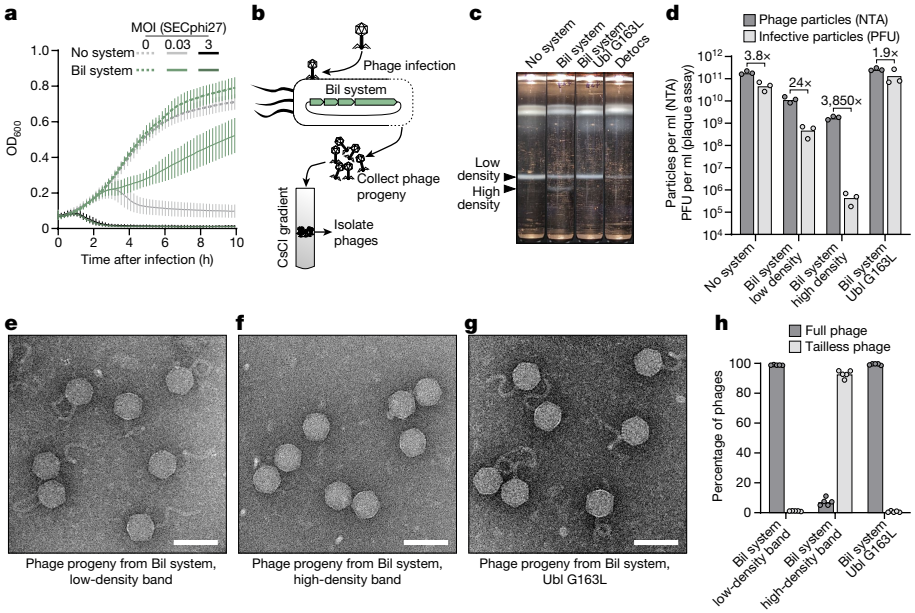


Fig. 2 | The Bil system causes the production of non-infective phage particles. **a**, Growth curves of *E. coli* expressing a control plasmid or the Bil system, either uninfected or infected with SECphi27 at a MOI of 0.03 or 3. The average with s.d. of three biological replicates is shown. **b**, Overview of the phage purification process. Bacteria expressing the Bil system were infected with SECphi27 at an MOI of 0.1 for 3 h to allow at least two full rounds of phage replication. To purify the resulting phages, they were isolated from CsCl gradients. **c**, Photographs of CsCl gradients loaded with phages obtained from bacteria expressing the indicated systems. Only the wild-type Bil system leads to the appearance of a second, higher-density band of phages. Detocs is an unrelated defence system that protects against SECphi27 and is presented as control[28]. **d**, Particle concentration and number of PFUs of phages obtained as shown in **c**, measured by NTA and plaque assays, respectively. Bars represent the average of three biological replicates with individual data points overlaid. Fold difference between number of particles and number of infective particles is presented for each condition. **e**–**g**, Representative negative staining transmission electron microscopy images of phages obtained from the low-density (**e**) or high-density (**f**) bands of bacteria expressing the wild-type Bil system or the band from bacteria expressing the mutant Bil system (**g**). Scale bars, 100 nm. **h**, Quantification of full and tailless phage particles with DNA-filled capsids observed in electron microscopy experiments shown in **e**–**g**. Total number of phages quantified are: Bil system, low-density band, $n = 2{,}566$; Bil system, high-density band, $n = 496$; Bil system Ubl G163L, $n = 1{,}670$. Bars represent the average of five separately quantified grid regions with individual data points overlaid.

those observed for abortive infection (Abi) defence systems, which function by inducing death of infected cells at a time point earlier than that necessary for completion of the phage replication cycle[22]. However, cells expressing the Bil system that were infected at high MOI lysed at the same time as control cells rather than lysing at an earlier time point as expected for Abi systems[22] (Fig. 2a). This observation pointed to the possibility that the Bil system allows the phages to complete their temporally controlled replication cycle, but still somehow prevents the production of infective phage progeny.

To examine whether phage progeny emerge from infected Bil-expressing cultures, we collected filtered supernatants from Bil-expressing cells that were lysed following infection with SECphi27. We then used isopycnic CsCl gradient centrifugation to achieve a concentrated phage preparation (Fig. 2b). Mature phages concentrated in a CsCl gradient typically localize to a single band where the density of phage particles matches the local density of the gradient[23]. However, supernatant derived from infected Bil-expressing cells formed two distinct bands on the CsCl gradient (Fig. 2c). One of these bands was at the same density in the gradient as the band derived from phages propagated on control cells, suggesting that this band represents mature phages. The second band was closer to the bottom of the gradient and hence represented particles of higher density. This second band was not observed for phages propagated on a mutant Bil system, suggesting that generation of higher-density particles is a property of a functional Bil system (Fig. 2c).

We next quantified the phages isolated from each band in the CsCl gradient using nanoparticle tracking analysis (NTA), a biophysical technique that can count particles with diameters of 10–1,000 nm by tracking their Brownian motion[24]. Using the same phage samples, we quantified the number of infective particles (plaque-forming units, PFUs) using standard plaque assays on an indicator strain. For phages propagated on control cells or on cells expressing the mutant Bil system, the number of particles measured by the biophysical NTA technique was largely in agreement with the measured PFUs, confirming that the NTA method is suitable for accurately counting virions[25] (Fig. 2d). By contrast, the number of particles measured in the unique high-density band derived from cells expressing the Bil system was roughly 4,000-fold greater than the PFUs measured for the same sample, indicating that more than 99.9% of particles in this band were non-infective (Fig. 2d). Similar measurements for the low-density band derived from infected Bil-expressing cells, which presumably includes mature phages, showed that this band contained 24 times more particles measured by NTA than PFUs, suggesting that even in the low-density band, most particles are non-infective (Fig. 2d).

To further characterize the phages emerging from bacteria expressing the Bil system, we performed negative staining transmission electron microscopy on particles derived from each of the two bands of the CsCl gradient. Phages from the low-density band were morphologically indistinct from normal phages, possessing tails and DNA-filled capsids typical for the SECphi27 siphovirus (Fig. 2e,h). By contrast, particles from the high-density band mostly consisted of head-only, DNA-filled capsids without a tail (Fig. 2f,h), explaining why these particles were not infective (Fig. 2d). Consistent with this observation, our NTA measurements showed that particles from the high-density band were of substantially smaller size (Extended Data Fig. 3a–e). This observation explains why these tailless phages form a denser band in the CsCl gradient: the removal of the tail increases the ratio of DNA to protein within the particle, which in turn increases its buoyant density[26,27]. As expected, phages propagated on the mutated version of the Bil system showed normal morphology (Fig. 2g,h). These results show that the Bil

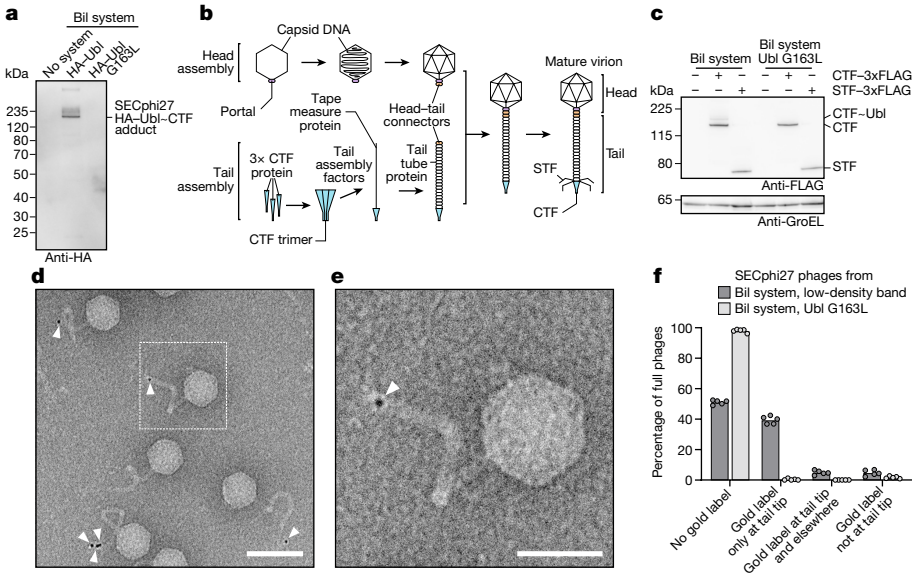


Fig. 3 | The phage CTF is the target of the Bil system. a, Immunoprecipitation of HA-tagged Ubl protein from SECphi27 phages collected following infection of bacteria expressing wild-type or mutant Bil systems, analysed by western blotting. Only one phage protein, the CTF of SECphi27, is revealed to be conjugated to HA–Ubl. A representative image of three biological replicates is shown. **b**, Simplified representation of the siphophage virion assembly pathway, based on studies of phage λ (refs. 14,29,30). **c**, Co-expression of the Bil system with either the CTF or the side tail fibre (STF) of SECphi27, analysed by western blotting. GroEL was used as loading control on the same blot. A representative image of three biological replicates is shown. Quantification of the percentage of Ubl-conjugated CTF is detailed in Extended Data Fig. 4c. **d**, Representative immunogold labelling transmission electron microscopy image of SECphi27 phages propagated on bacteria expressing the HA–Ubl Bil system and isolated from the low-density band of the CsCl gradient. White arrowheads represent gold labelling of HA–Ubl. Scale bar, 100 nm. See Extended Data Fig. 5 for more images. **e**, Magnification of the dashed area in **d**. White arrowhead represents gold labelling of HA–Ubl. Scale bar, 50 nm. **f**, Quantification of gold-labelled tailed phage particles observed in electron microscopy experiments shown in **d** and in Extended Data Fig. 6a. Total number of phages quantified are: Bil system, low-density band, $n = 1{,}753$; Bil system Ubl G163L, $n = 1{,}239$. Bars represent the average of five separately quantified grid regions with individual data points overlaid.

system somehow interferes with phage assembly, causing the generation of tailless phages as well as tailed phages with reduced infectivity.

To rule out the possibility that the production of partially assembled phages is a general property of antiphage defence systems that protect against SECphi27, we propagated SECphi27 on *E. coli* cells expressing Detocs, a defence system that depletes cellular ATP in response to infection, thus aborting the phage replication cycle[28]. Propagation of SECphi27 on Detocs-expressing cells yielded fewer phage progeny, consistent with previous observations that Detocs protects against this phage[28] (Fig. 2c). However, SECphi27 progeny obtained from Detocs-expressing bacteria ran as a single band on the CsCl gradient, and the denser band observed for phages derived from the Bil system was not visible for Detocs-derived phages (Fig. 2c). These results further indicate that the production of tailless phages is a unique property of the Bil defence system.

The CTF is the target of the Bil system

Although it is obvious why tailless phages would be non-infective, it remained unclear why Bil-derived phages from the low-density CsCl band, which seemed properly assembled and tailed according to electron microscopy examination, still showed reduced infectivity (Fig. 2d,e). On the basis of the properties of the Bil system, we proposed that these phages might have been conjugated to the Bil Ubl protein in a way that interferes with their infectivity. To test this hypothesis, we experimented with a Bil system variant in which the BilA Ubl protein was N-terminally fused to an HA tag. This tagged system showed defence against phage SECphi27, indicating that N-terminal tagging of the Ubl protein does not interfere with the function of the Bil system (Extended Data Fig. 4a). We then propagated phages on cells expressing the tagged Bil system, isolated these phages using CsCl gradients and immunoprecipitated the phages using anti-HA antibodies. Western blot analysis of proteins from pulled-down phages revealed a major band at roughly 150 kDa, indicating a single phage protein conjugated to the Ubl (Fig. 3a). Only one protein of SECphi27, the CTF, is large enough to generate a protein band of this size (CTF roughly 132 kDa; HA–Ubl roughly 19 kDa). Mass spectrometry analysis identified the SECphi27 CTF as well as the Ubl protein in this band (Supplementary Table 1), showing that the 150 kDa band indeed represents a Ubl-CTF adduct. These results indicate that the Bil system conjugates its Ubl to the phage CTF.

The CTF (also called the spike protein or tip attachment protein) is an essential structural component of many siphophages, forming the tip of the tail in the mature virion (Fig. 3b). The CTF contains the receptor-binding domain of the phage, which is responsible for host receptor recognition[15]. Furthermore, the CTF is essential for assembly of the phage tail[14,29,30]. In phage λ, for which the tail assembly cascade was studied in detail, it was shown that tail assembly begins from trimerization of the CTF. The CTF trimer then recruits tail assembly factors, which in turn recruit the tail tape measure protein, initiating the polymerization of the tail tube proteins. Once the tail is mature, it is attached to the DNA-filled capsid, which is assembled in the cell independently of the tail, to ultimately produce the mature tailed virion[14,29,30] (Fig. 3b). Therefore, conjugation of a Ubl protein to the CTF might interfere with assembly of the phage tail, explaining why many of the virions emerging from infected Bil-expressing cells are tailless. In support of this hypothesis, pull-down attempts of the fraction of tailless phages (high-density CsCl band) that were propagated on the HA–Ubl Bil system did not retrieve any tagged proteins (Extended Data Fig. 4b), because the CTF is missing from these tailless phages.

To confirm that the Bil system specifically targets the phage CTF, we co-expressed a 3xFLAG-tagged version of the CTF together with the Bil system in the absence of other phage components, and then analysed whole cell lysates using western blotting. This revealed two bands: one corresponding to the unmodified CTF, and one to the Ubl-CTF adduct

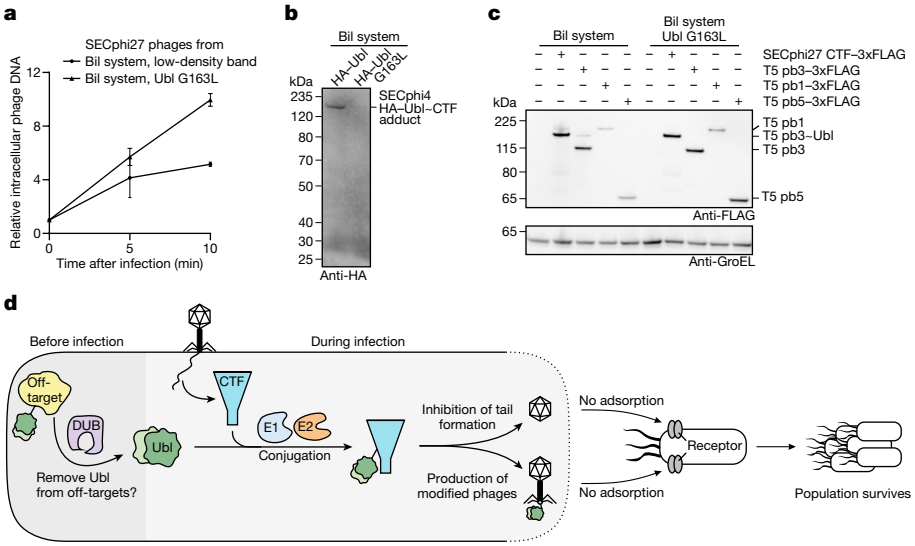


Fig. 4 | The Bil defence system targets tail tip proteins of distantly related phages. a, Ratio of SECphi27 DNA to bacterial DNA during infection. Bacteria were infected at MOI = 1, on the basis of NTA phage particle quantification. Total DNA was extracted at the indicated time points and quantified by qPCR. The *y* axis represents relative phage DNA amounts compared to bacterial DNA amounts, normalized to the value at $t = 0$ min after infection. Average of three biological experiments. Error bars show average with s.d. **b**, Immunoprecipitation of HA-tagged Ubl protein from SECphi4 phages collected following infection of bacteria expressing wild-type or mutant Bil systems, analysed by western blotting. Only the CTF of SECphi4 is revealed to be conjugated to HA–Ubl. A representative image of three biological replicates is shown. **c**, Co-expression of the Bil system with either the CTF of SECphi27, the baseplate hub protein pb3 of T5, the L-shaped tail fibre protein pb1 of T5 or the receptor-binding tail protein pb5 of T5, analysed by western blotting. GroEL was used as loading control on the same blot. Higher exposure of the same blot is presented in Extended Data Fig. 8b. A representative image of two biological replicates is shown. **d**, Model for the mechanism of action of the Bil defence system. After phage infection, the Bil system conjugates its Ubl protein to the CTF of the phage by means of the E1 and E2 enzymes, leading either to the inhibition of tail formation and generation of tailless phages or to the production of modified phages with obstructed tail tips. After host lysis by the phage, these two phage populations are released but are unable to adsorb and inject their DNA into the host, thereby preventing the next infection cycle. Before infection, the Ubl may get conjugated to cellular off-targets, which can be reversed by the DUB.

(Fig. 3c and Extended Data Fig. 4c). By contrast, when we expressed the CTF with the mutant Bil system, only the unmodified CTF could be observed (Fig. 3c). To further examine whether the Bil system is specific to the CTF, we performed the same experiment with the side tail fibre of the phage, which is also localized at the distal part of the tail (Fig. 3b), but could not observe conjugation of the Ubl to the side tail fibre (Fig. 3c). These results further substantiate that the Bil system specifically conjugates the Ubl to the phage CTF protein.

To further test whether the fraction of fully assembled, tailed phages that emerged from infected Bil-expressing cells are specifically modified by the Ubl on their CTF, we performed immunogold labelling transmission electron microscopy experiments. In these experiments, phages propagated on a Bil system with an HA-tagged Ubl and isolated from the low-density band of the CsCl gradient were probed with anti-HA antibodies and then with secondary antibodies attached to 6 nm colloidal gold particles. In agreement with our biochemical data, for most of the gold-labelled phage particles, labelling was observed exclusively at the tip of the phage tails: the position of the CTF (Fig. 3d–f and Extended Data Fig. 5). We occasionally noted two gold particles, and sometimes more, at the same tail tip, possibly representing Ubl conjugation on two or three monomers of the CTF trimer or representing several secondary antibodies bound to the same anti-HA primary antibody (Extended Data Fig. 5). The same experiment with a tagged but mutated Ubl protein did not lead to labelling of the tail tip (Fig. 3f and Extended Data Fig. 6a). These results demonstrate that the Bil system attaches the Ubl protein to the CTF protein of the phage.

As the CTF contains the receptor-binding domain of the phage, we proposed that conjugation of Ubl to the phage CTF might interfere with the ability of the phage to adsorb and inject its DNA to the bacterial host. To test this hypothesis, we collected phages from infected bacterial cultures either expressing the wild-type or the mutant Bil system. We then used these phages to infect Bil-lacking bacteria, and measured the amount of intracellular phage DNA shortly after infection to estimate successful DNA injection. In support of our hypothesis, substantially less DNA accumulated in cells infected by Bil-derived phages, indicating that Ubl conjugation to the CTF inhibits DNA injection (Fig. 4a). In further support for this observation, efficiency of centre of infection experiments showed substantially lower centres of infection for phages from Bil-expressing bacteria as compared to control phages (Extended Data Fig. 6b). These results indicate that phages that are Ubl-tagged by the Bil system are less infective due to impaired ability to adsorb and inject their DNA into the bacterial host.

CTFs of distant phages are targeted

The Bil system defends against phages spanning many different taxonomical families[13]. To test whether the system protects against diverse phages by the same mechanism, we selected SECphi4, a siphophage from the *Dhillonvirus* genus whose genome (roughly 45 kb) has no detectable sequence similarity to the genome of SECphi27 (roughly 52 kb) and against which the Bil system strongly defends (Extended Data Fig. 7a). We purified SECphi4 phages propagated on a strain expressing the HA–Ubl-tagged Bil system and immunoprecipitated these phages with anti-HA antibodies. Western blot analysis of proteins from immunoprecipitated phages revealed only one SECphi4 protein that was conjugated to the Ubl (Fig. 4b). Mass spectrometry analysis identified this protein band as an adduct of the CTF of SECphi4 and the Ubl of the Bil system (Supplementary Table 2). In support of this observation, co-expression of a tagged version of the CTF of SECphi4 with the Bil system in the absence of phage infection showed that the system can conjugate the Ubl protein to the SECphi4 CTF (Extended Data Fig. 7b). These results demonstrate that the Bil system functions similarly when

protecting against distantly related phages, and that the phage CTF is the target of the Bil system for Ubl conjugation.

Whereas SECphi27 and SECphi4 have no sequence similarity on the nucleotide level, 16 of the 85 (roughly 19%) predicted proteins in the SECphi27 proteome show homology to proteins of SECphi4 (Supplementary Table 3). Notably, 11 of these 16 proteins are predicted tail structure proteins or tail assembly proteins, including the CTF, suggesting that these two phages possess similar tail structures (Supplementary Table 3). The CTF proteins of SECphi4 and SECphi27 show roughly 34% sequence identity on the amino acid level, and prediction of their protein structures using AlphaFold2 revealed substantial structural similarities between the two proteins (Extended Data Fig. 7c), which could explain how the Bil system may recognize both proteins and defend against phages from different families. The fact that two distantly related phages that share little but their tail structures are both targeted by the Bil system further supports that the primary mechanism of the Bil system involves interfering with phage tail assembly by conjugating a Ubl protein on the phage CTF.

The Bil system also defends against T5 (ref. 13), a siphophage with a tail structure different from that of SECphi27 and SECphi4 (ref. 31). Despite the differences in tail structure, the N-terminal half of the SECphi27 CTF shows structural similarity to the T5 baseplate hub protein pb3, a central structural protein of the T5 tail tip (Extended Data Fig. 8a). To test whether pb3 can be targeted by the Bil system, we co-expressed the Bil system with 3xFLAG-tagged pb3 (roughly 110 kDa) and analysed whole cell lysates using western blotting. This analysis showed that pb3 became conjugated to the Ubl protein, as indicated by the second roughly 130 kDa band that was absent in samples obtained from the mutant Bil system (Fig. 4c and Extended Data Fig. 8b). By contrast, we did not observe conjugation to pb1 (L-shaped tail fibre) or pb5 (receptor-binding tail protein), two structural proteins of T5 that are located at the tail tip as well[31], demonstrating the specificity of the Bil system to the T5-encoded homologue of SECphi27 CTF.

Discussion

In this study, we investigated the mechanism of immunity provided by a bacterial defence system capable of conjugating an ISG15-like Ubl protein. Our data support a model in which this system specifically conjugates the ubiquitin-like protein to the CTF of the phage (Fig. 4d). This conjugation can prevent tail assembly and lead to the generation of non-infective tailless phages or produce infection-impaired tailed phages whose tail tip is obstructed by a covalently attached Ubl. This mode of action does not save the infected cell from eventually being lysed by the phage, but as the particles that emerge from the lysed cell are mostly non-infective, the Bil system ends up protecting the surrounding bacteria from the spread of phage epidemic (Fig. 4d). The mechanism of the Bil system is different from that of abortive infection (Abi) systems, which actively kill the infected cells once phage infection is detected[32,33]. However, a similar outcome of culture-level protection is achieved by both Bil and Abi systems.

Whereas our results show the tail tip structure as the target of the Bil system, the mechanism of target recognition remains to be studied. Our observations using taxonomically distant phages suggest that a structural motif in the tail tip structure may be the determining factor of recognition (Fig. 4b,c and Extended Data Figs. 7b,c and 8a). This fold is also present in the baseplate hub protein gp27 of T-even phages (Extended Data Fig. 8c). However, we did not observe conjugation of the Ubl protein to gp27 of phage T6 following co-expression of this protein with the Bil system (Extended Data Fig. 8d). Because gp27 is located in the core of the complex baseplate structure of T-even phages[34], it is possible that other structural proteins are needed either for proper folding of gp27 or for its recognition by the Bil system. Alternatively, the Bil system might target more phage or host proteins to exert its defensive activity. Such redundant targeting could also explain why we were not able to isolate phage mutants that escape defence by the Bil system.

An aspect of the Bil system that was not studied here in detail is the role of the DUB protein. This protein is essential for the proper activity of the system, as disruption of its active site renders the system inactive (Fig. 1d and Extended Data Fig. 1b). It is possible that the DUB removes the Ubl from proteins when non-specific conjugations occur to keep a pool of free Ubl until phage infection. Indeed, a Bil system mutated in the DUB was able to defend against SECphi27 when the Ubl was overexpressed from a second plasmid (Extended Data Fig. 9a). Moreover, overexpression of the Ubl together with the wild-type Bil system increased defence against SECphi27 and SECphi18, whereas overexpression of the mutated Ubl reduced defence. This suggests that the pool of free Ubl may be a limiting factor for defence in these cases (Extended Data Fig. 9a). We did not observe this behaviour for SECphi4 or SECphi6, indicating that the DUB might have extra functions during infection by these phages (Extended Data Fig. 9a).

Our data show that the DUB of the *Collimonas* Bil system studied here can cleave the Ubl when it is fused to green fluorescent protein (GFP) (Extended Data Fig. 9b), which may suggest that activity of the DUB could prevent potential toxic effects of non-specific Ubl conjugation to bacterial proteins. However, we did not observe toxicity in strains expressing the Bil system with a mutated or deleted DUB (Extended Data Fig. 9c). A recent study showed that in a type II Bil system, the DUB processes the C terminus of the Ubl protein to expose the essential C-terminal glycine[20]. The DUB might also be necessary to release the Ubl from a storage position within the cell, as was recently shown for the cyclase protein of a type II CBASS defence system, which is conjugated to a membrane-associated protein and is released from that protein during infection by a CBASS-associated DUB[35]. Some siphophages encode tail assembly proteins containing DUB domains whose functions in phage tail assembly are not understood at present[36]. Because the Bil system interferes with phage tail assembly, it is tempting to speculate that the inclusion of DUB domains in phage tail assembly proteins is an antidefence measure to protect the phage from the action of the Bil system by cleaving the Ubl off the CTF.

Proteins with E1, E2 and DUB domains are also present as accessory proteins in the antiphage defence systems CBASS and Pycsar[37–39]. These systems depend on second messenger signalling molecules that are produced in response to phage detection, and it was shown that the proteins that generate the second messenger molecules can be conjugated by the E1 and E2 enzymes to unknown targets through a ubiquitin-like mechanism, thereby priming their enzymatic activity[40,41]. In contrast to the Bil system, E1/E2-dependent conjugation in CBASS is only essential for defence against some phages, and dispensable for others[37,40,41]. As the Ubl of the Bil system has no predicted enzymatic activity[13], it is likely that the primary function of the Bil system is to interfere with phage assembly and cause the generation of non-infective particles. It is possible that conjugation of CBASS proteins to phage structural components may be another aspect of CBASS defence.

The Bil system we studied is a representative of a large family of defence systems encoding E1, E2 and Ubl proteins[13]. In some of these systems, the Ubl contains a single ubiquitin-like domain (instead of the two fused domains in the Bil system), and in some cases, the gene with the DUB domain is missing[13]. It remains to be determined whether all these systems target the phage CTF, or whether some of them may target other components of the phage.

The Bil system can be viewed as analogous to the human ISG15 system, in the sense that both systems encode a double ubiquitin Ubl and dedicated Ubl conjugation machinery, and that both systems protect against viruses[3–5]. Despite extensive studies over the course of several decades, the mechanism of ISG15 antiviral defence is not entirely understood[3–5]. A variety of cellular and viral targets were suggested for ISG15 (ref. 5), and it was also suggested that the dedicated E1, E2 and E3 enzymes of ISG15 non-specifically conjugate it to newly synthesized

proteins in infected cells to interfere with viral reproduction[42]. Our discovery that the bacterial analogue of the human ISG15 interferes with phage assembly by targeting viral structural proteins may guide future studies on the human counterpart.

Online content

Any methods, additional references, Nature Portfolio reporting summaries, source data, extended data, supplementary information, acknowledgements, peer review information; details of author contributions and competing interests; and statements of data and code availability are available at https://doi.org/10.1038/s41586-024-07616-5.

1. Li, J., Chai, Q. Y. & Liu, C. H. The ubiquitin system: a critical regulator of innate immunity and pathogen-host interactions. *Cell Mol. Immunol.* **13**, 560–576 (2016).
2. Hu, H. & Sun, S. C. Ubiquitin signaling in immune responses. *Cell Res.* **26**, 457–483 (2016).
3. Dzimianski, J. V., Scholte, F. E. M., Bergeron, É. & Pegan, S. D. ISG15: it's complicated. *J. Mol. Biol.* **431**, 4203–4216 (2019).
4. Freitas, B. T., Scholte, F. E. M., Bergeron, É. & Pegan, S. D. How ISG15 combats viral infection. *Virus Res.* **286**, 198036 (2020).
5. Perng, Y. C. & Lenschow, D. J. ISG15 in antiviral immunity and beyond. *Nat. Rev. Microbiol.* **16**, 423–439 (2018).
6. Kerscher, O., Felberbaum, R. & Hochstrasser, M. Modification of proteins by ubiquitin and ubiquitin-like proteins. *Annu. Rev. Cell Dev. Biol.* **22**, 159–180 (2006).
7. Mevissen, T. E. T. & Komander, D. Mechanisms of deubiquitinase specificity and regulation. *Annu. Rev. Biochem.* **86**, 159–192 (2017).
8. Clague, M. J. & Urbé, S. Ubiquitin: same molecule, different degradation pathways. *Cell* **143**, 682–685 (2010).
9. Der, S. D., Zhou, A., Williams, B. R. & Silverman, R. H. Identification of genes differentially regulated by interferon alpha, beta, or gamma using oligonucleotide arrays. *Proc. Natl Acad. Sci. USA* **95**, 15623–15628 (1998).
10. Sgorbissa, A. & Brancolini, C. IFNs, ISGylation and cancer: Cui prodest? *Cytokine Growth Factor Rev.* **23**, 307–314 (2012).
11. Mayo-Muñoz, D., Pinilla-Redondo, R., Birkholz, N. & Fineran, P. C. A host of armor: prokaryotic immune strategies against mobile genetic elements. *Cell Rep.* **42**, 112672 (2023).
12. Georjon, H. & Bernheim, A. The highly diverse antiphage defence systems of bacteria. *Nat. Rev. Microbiol.* **21**, 686–700 (2023).
13. Millman, A. et al. An expanded arsenal of immune systems that protect bacteria from phages. *Cell Host Microbe* **30**, 1556–1569.e5 (2022).
14. Rajagopala, S. V., Casjens, S. & Uetz, P. The protein interaction map of bacteriophage lambda. *BMC Microbiol.* **11**, 213 (2011).
15. Wang, J., Hofnung, M. & Charbit, A. The C-terminal portion of the tail fiber protein of bacteriophage lambda is responsible for binding to LamB, its receptor at the surface of *Escherichia coli* K-12. *J. Bacteriol.* **182**, 508–512 (2000).
16. Jumper, J. et al. Highly accurate protein structure prediction with AlphaFold. *Nature* **596**, 583–589 (2021).
17. Deol, K. K., Lorenz, S. & Strieter, E. R. Enzymatic logic of ubiquitin chain assembly. *Front. Physiol.* **10**, 835 (2019).
18. Termathe, M. & Leidel, S. A. The Uba4 domain interplay is mediated via a thioester that is critical for tRNA thiolation through Urm1 thiocarboxylation. *Nucleic Acids Res.* **46**, 5171–5181 (2018).
19. Evans, R. et al. Protein complex prediction with AlphaFold-Multimer. Preprint at *bioRxiv* https://doi.org/10.1101/2021.10.04.463034 (2022).
20. Chambers, L. R. et al. A eukaryotic-like ubiquitination system in bacterial antiviral defence. *Nature* https://doi.org/10.1038/s41586-024-07730-4 (2024).
21. Hensel, Z. A plasmid-based *Escherichia coli* gene expression system with cell-to-cell variation below the extrinsic noise limit. *PLoS ONE* **12**, e0187259 (2017).
22. Rousset, F. & Sorek, R. The evolutionary success of regulated cell death in bacterial immunity. *Curr. Opin. Microbiol.* **74**, 102312 (2023).
23. Bachrach, U. & Friedmann, A. Practical procedures for the purification of bacterial viruses. *Appl. Microbiol.* **22**, 706–715 (1971).
24. Filipe, V., Hawe, A. & Jiskoot, W. Critical evaluation of nanoparticle tracking analysis (NTA) by NanoSight for the measurement of nanoparticles and protein aggregates. *Pharm. Res.* **27**, 796–810 (2010).
25. Kramberger, P., Ciringer, M., Štrancar, A. & Peterka, M. Evaluation of nanoparticle tracking analysis for total virus particle determination. *Virol. J.* **9**, 265 (2012).
26. Meselson, M., Stahl, F. W. & Vinograd, J. Equilibrium sedimentation of macromolecules in density gradients. *Proc. Natl Acad. Sci. USA* **43**, 581–588 (1957).
27. Quillin, M. L. & Matthews, B. W. Accurate calculation of the density of proteins. *Acta Crystallogr. D Biol. Crystallogr.* **56**, 791–794 (2000).
28. Rousset, F. et al. A conserved family of immune effectors cleaves cellular ATP upon viral infection. *Cell* **186**, 3619–3631.e13 (2023).
29. Katsura, I. & Kühl, P. W. Morphogenesis of the tail of bacteriophage lambda. III. Morphogenetic pathway. *J. Mol. Biol.* **91**, 257–273 (1975).
30. Xu, J., Hendrix, R. W. & Duda, R. L. Chaperone-protein interactions that mediate assembly of the bacteriophage lambda tail to the correct length. *J. Mol. Biol.* **426**, 1004–1018 (2014).
31. Linares, R. et al. Structural basis of bacteriophage T5 infection trigger and *E. coli* cell wall perforation. *Sci. Adv.* **9**, eade9674 (2023).
32. Lopatina, A., Tal, N. & Sorek, R. Abortive infection: bacterial suicide as an antiviral immune strategy. *Annu. Rev. Virol.* **7**, 371–384 (2020).
33. Aframian, N. & Eldar, A. Abortive infection antiphage defense systems: separating mechanism and phenotype. *Trends Microbiol.* **31**, 1003–1012 (2023).
34. Kostyuchenko, V. A. et al. Three-dimensional structure of bacteriophage T4 baseplate. *Nat. Struct. Biol.* **10**, 688–693 (2003).
35. Krüger, L. et al. Reversible conjugation of a CBASS nucleotide cyclase regulates bacterial immune response to phage infection. *Nat. Microbiol.* **9**, 1579–1592 (2024).
36. Iyer, L. M., Burroughs, A. M. & Aravind, L. The prokaryotic antecedents of the ubiquitin-signaling system and the early evolution of ubiquitin-like beta-grasp domains. *Genome Biol.* **7**, R60 (2006).
37. Cohen, D. et al. Cyclic GMP-AMP signalling protects bacteria against viral infection. *Nature* **574**, 691–695 (2019).
38. Millman, A., Melamed, S., Amitai, G. & Sorek, R. Diversity and classification of cyclic-oligonucleotide-based anti-phage signalling systems. *Nat. Microbiol.* **5**, 1608–1615 (2020).
39. Tal, N. et al. Cyclic CMP and cyclic UMP mediate bacterial immunity against phages. *Cell* **184**, 5728–5739.e16 (2021).
40. Ledvina, H. E. et al. An E1-E2 fusion protein primes antiviral immune signalling in bacteria. *Nature* **616**, 319–325 (2023).
41. Jenson, J. M., Li, T., Du, F., Ea, C. K. & Chen, Z. J. Ubiquitin-like conjugation by bacterial cGAS enhances anti-phage defence. *Nature* **616**, 326–331 (2023).
42. Durfee, L. A., Lyon, N., Seo, K. & Huibregtse, J. M. The ISG15 conjugation system broadly targets newly synthesized proteins: implications for the antiviral function of ISG15. *Mol. Cell* **38**, 722–732 (2010).
43. Vijay-Kumar, S., Bugg, C. E. & Cook, W. J. Structure of ubiquitin refined at 1.8 A resolution. *J. Mol. Biol.* **194**, 531–544 (1987).

Publisher's note Springer Nature remains neutral with regard to jurisdictional claims in published maps and institutional affiliations.

Springer Nature or its licensor (e.g. a society or other partner) holds exclusive rights to this article under a publishing agreement with the author(s) or other rightsholder(s); author self-archiving of the accepted manuscript version of this article is solely governed by the terms of such publishing agreement and applicable law.

© The Author(s), under exclusive licence to Springer Nature Limited 2024

Methods

Bacterial strains and phages

The Bil system (IMG[44] gene IDs: BilA, 2609810443; BilB, 2609810442; BilC, 2609810441; BilD, 2609810440) and its mutant variants were expressed in *E. coli* MG1655. A plasmid containing *gfp* instead of the Bil system was used as negative control throughout this study (denoted 'no system'). Bacteria were grown in MMB (Luria-Bertani medium supplemented with 0.1 mM $MnCl_2$ and 5 mM $MgCl_2$) at 25 °C with shaking at 200 rpm, and the appropriate antibiotics (100 μg ml^{-1} ampicillin and/or 30 μg ml^{-1} chloramphenicol) were added. *Caulobacter* sp. Root343 was grown in tryptic soy broth at 28 °C with shaking at 200 rpm. The bacterial strains and phages used in this study are listed in Supplementary Table 4. Infection was performed in MMB with or without 0.5% agar.

Plasmid and strain construction

All plasmids with their respective inserts used in this study are listed in Supplementary Table 5. Variants of the Bil system were generated by amplification of the plasmid containing the wild-type Bil system[13] using primers that contained the desired modification followed by treatment with KLD enzyme mix (NEB) according to the manufacturer's instructions to obtain transformable plasmids. Plasmids encoding phage proteins were constructed by amplification of the desired genes from the phage genomes and assembly into the pBbA6c backbone using NEBuilder HiFi DNA Assembly Master Mix (NEB) according to the manufacturer's instructions. Tetracycline-inducible variants of the Bil system were constructed by amplification of the desired Bil system from the arabinose-inducible plasmids and assembled into the pBbA2k backbone as above. After sequence verification, plasmids were transformed into *E. coli* MG1655 using transformation and storage solution[45].

Plaque assays

To test the defensive properties of the Bil system and its mutant versions, the small drop plaque assay was used[46]. Here, 300 μl of an overnight culture of bacteria containing the respective version of the Bil system or the negative control strain were mixed with 30 ml of melted 0.5% MMB agar containing 0.2% arabinose. The mixture was poured into a 12 cm square plate and left to solidify for 1 h at room temperature. Tenfold serial dilutions of phages in MMB were prepared and 10 μl drops of each dilution were plated on the bacterial layer. The plates were incubated overnight at 25 °C. PFUs were counted after overnight incubation.

Liquid infection assays

Overnight cultures of bacteria were diluted 1:100 in MMB and incubated until they reached an optical density at 600 nm (OD_{600}) of 0.3, after which 180 μl of the culture was transferred into a 96-well plate containing 20 μl of either MMB (for the uninfected control) or phage lysate for a final MOI of 3 or 0.03. Plates were incubated at 25 °C with shaking in a Tecan Infinite 200 plate reader and the OD_{600} was measured every 10 min. Infections were performed in biological triplicates in three separate plates with technical triplicates in each plate. Three wells were filled with medium in each plate to serve as the blank, which was subtracted from the OD_{600} values of the wells containing bacteria.

Growth curve assays

Growth curve experiments were performed like the liquid infection assays described above, except that bacteria were diluted 1:100 in the 96-well plate and their growth measured as described above.

Phage purification

To purify phages for electron microscopy and NTA, 25 ml cultures of bacteria were grown with the appropriate antibiotics and 0.2% arabinose at 25 °C with shaking until they reached an OD_{600} of 0.55. Then, the cultures were infected with phages at an MOI of 0.1, followed by incubation at 25 °C for 3 h with shaking to allow for at least two full rounds of phage replication. To clear the cultures of unlysed bacteria and debris, they were centrifuged at 3,300*g* and 4 °C for 10 min and filtered through a 0.2 μm filter. Then 12.5 ml of 20 mM Tris-HCl, pH 7.5, 3 M NaCl, 30% PEG-8000 was added to the cleared phage lysates to precipitate the phages overnight at 4 °C. The precipitated phages were collected by centrifugation at 25,000*g* and 4 °C for 30 min, followed by decanting of the supernatant and centrifugation at 10,000*g* and 4 °C for 2 min. The remaining supernatant was removed and the phage pellets were soaked in 1 ml of 50 mM Tris-HCl, pH 7.5, 150 mM NaCl, 10 mM $MgSO_4$ on ice for 30 min to loosen them. The phage pellets were finally dissolved in the added buffer by careful pipetting and loaded on CsCl step gradients (1 ml of $\rho = 1.3$, 4 ml of $\rho = 1.4$, 4 ml of $\rho = 1.5$, 1 ml of $\rho = 1.7$; all in 50 mM Tris-HCl, pH 7.5, 10 mM $MgSO_4$) formed in open-top polyclear ultracentrifugation tubes (Seton Scientific). The gradients were centrifuged in an SW41 rotor (Beckman) at 25,000 rpm and 4 °C for 3 h and the phage bands collected by needle side-puncture. The extracted phages were dialysed against 20 mM Tris-HCl, pH 7.5, 150 mM NaCl, 10 mM $MgSO_4$ overnight at 4 °C using Pur-A-Lyzer Maxi 12000 dialysis tubes (Sigma Aldrich). The phages were further concentrated by centrifugation in a TLA-110 rotor (Beckman) at 45,000 rpm and 4 °C for 1 h. After removal of the supernatant, the phages were soaked in 50 μl of 20 mM Tris-HCl, pH 7.5, 150 mM NaCl, 10 mM $MgSO_4$ on ice for 30 min, followed by careful resuspension to obtain the final samples.

Immunoprecipitation

For immunoprecipitation of HA-tagged Ubl from whole cell lysates (Fig. 1e), 50 ml of each strain was grown at 25 °C to an OD_{600} of 0.3 with 0.2% arabinose, followed by centrifugation at 3,300*g* and 4 °C for 10 min to pellet the bacteria. The supernatant was discarded and the pellet frozen at −80 °C. The pellet was thawed on ice and dissolved in 750 μl of tris-buffered saline with Tween (TBS-T) (20 mM Tris-HCl, pH 7.5, 150 mM NaCl, 0.05% Tween 20), followed by transfer to a 2 ml tube with lysing matrix E (MP Biomedicals) and mechanical lysis using a FastPrep-24 instrument (MP Biomedicals) at 6 m s^{-1} and 4 °C for 40 s. The lysate was cleared by centrifugation at 13,000*g* and 4 °C for 10 min. Next, 25 μl of anti-HA magnetic beads (Thermo Scientific) was washed with 1 ml of ice-cold TBS-T and the cleared lysate was added to the washed beads, followed by rotation at 4 °C for 1 h to allow binding of HA–Ubl to the beads. The lysate was removed and the beads washed three times with 500 μl ice-cold TBS-T for 1 min. The beads were washed with 500 μl of water and finally resuspended in 35 μl 1× Bolt LDS Sample Buffer (Thermo Scientific), 20 μl of which was subjected to non-reducing SDS–PAGE.

For immunoprecipitation of HA-tagged Ubl from isolated phages (Figs. 3a and 4b and Extended Data Fig. 4b), phages were purified as described above, except that the final concentration step after dialysis was skipped. Phages were added to 25 μl of washed beads and immunoprecipitation performed as described above. The beads were resuspended in 35 μl 1× Bolt LDS Sample Buffer supplemented with 50 mM DTT, of which 10 μl was used for western blotting and 20 μl was subjected to SDS–PAGE and mass spectrometry.

Analysis of Ubl~E1/E2 complex formation

To analyse covalent thioester-based complexes between the Ubl and E1/E2 proteins (Extended Data Fig. 1d,h), 10 ml of each strain was grown to an OD_{600} of 0.5 or 0.8 with 0.2% arabinose to express the Bil system. An equivalent to 0.1 OD_{600} of cells was collected and centrifuged at 13,000*g* and 4 °C for 2.5 min to pellet the bacteria. The pellet was resuspended in 100 μl 1× Bolt LDS Sample Buffer, which was split into two tubes. One of the tubes was supplemented with 50 mM DTT to achieve reducing conditions able to break potential thioester bonds[18]. Finally, 10 μl each of the reduced and the non-reduced samples were subjected to western blotting.

Co-expression analysis

For co-expression analyses (Figs. 3c and 4c and Extended Data Figs. 7b and 8d), 10 ml of each strain was grown to an OD_{600} of 0.5 with 0.2% arabinose to express the Bil system or the Ubl–GFP fusion protein. Then, the phage proteins or the DUB were induced with 0.1 mM IPTG or 50 ng ml^{-1} aTc, respectively, for 30 min. An equivalent of 0.1 OD_{600} of cells was collected and centrifuged at 13,000*g* and 4 °C for 2.5 min to pellet the bacteria. The pellet was resuspended in 100 µl 1× Bolt LDS Sample Buffer supplemented with 50 mM DTT, of which 10 µl were subjected to western blotting.

Gel electrophoresis and western blotting

For protein analysis, the indicated amounts of protein sample were boiled at 95 °C for 3 min and separated by 4–12% Bis-Tris SDS–PAGE (Thermo Scientific) either in 1× MES buffer (Thermo Scientific) or 1× MOPS buffer (Thermo Scientific) to resolve smaller and larger proteins, respectively, at 200 V. Coomassie staining was performed by addition of InstantBlue Coomassie Protein Stain (Abcam) for 1 h, followed by destaining with water. For western blotting, the gel was transferred to a polyvinyl difluoride membrane (Thermo Scientific) for 1 h at 20 V in 1× transfer buffer (Thermo Scientific) and probed with the appropriate primary antibody diluted in TBS-T with 3% BSA: rabbit anti-HA (Sigma Aldrich, catalogue no. H6908; 1:3,000 dilution), mouse anti-FLAG (Sigma Aldrich, catalogue no. F1804; 1:10,000 dilution), mouse anti-GFP (Sigma Aldrich, catalogue no. 11814460001; 1:5,000 dilution) or HRP-conjugated Strep-Tactin (IBA catalogue no. 2-1502-001; 1:50,000 dilution). Visualization of the primary antibody was performed using HRP-conjugated goat anti-rabbit secondary antibody (Thermo Scientific, catalogue no. 31460; 1:10,000 dilution) or HRP-conjugated goat antimouse secondary antibody (Thermo Scientific, catalogue no. 31430; 1:10,000 dilution) and incubation with ECL solution (Merck Millipore). No secondary antibody was used in the case of the HRP-coupled Strep-Tactin. Where appropriate, the membranes were stripped using Restore PLUS Western Blot Stripping Buffer (Thermo Scientific) and probed with primary rabbit anti-GroEL antibody (Sigma Aldrich, catalogue no. G6532) as loading control. The percentage of Ubl-conjugated CTF was quantified using ImageJ[47] v.1.54d. The area under the curve of the conjugated band was divided by the sum of the areas under the curve of the conjugated plus the unconjugated band.

Mass spectrometry

To identify the phage proteins observed to be conjugated to HA–Ubl, SDS–PAGE was run and stained with Coomassie as described above. The band of interest was cut from the gel and the same area of the gel was cut for the control as well. The gel bands were subjected to in-gel tryptic digestion.

For identification of the Ubl-CTF adducts, the resulting peptides were analysed using nanoflow liquid chromatography (nanoAcquity) coupled to high resolution, high mass accuracy mass spectrometry (Q Exactive HF). Each sample was analysed on the instrument separately in a random order in discovery mode. The data were searched against the *E. coli* K-12 database appended with the SECphi27, SECphi4 and Bil system proteomes as well as common laboratory contaminants. Carbamidomethylation of C was set as a fixed modification, whereas oxidation of M and deamidation of NQ were defined as variable ones.

For identification of the proteins pulled down by the Ubl, the resulting peptides were analysed using NanoLC–MS/MS on an Orbitrap Fusion (Thermo Scientific) equipped with a PicoView Ion Source (New Objective) and coupled to an EASY-nLC 1000 (Thermo Scientific). Peptides were loaded on a trapping column (2 cm × 150 µm ID, PepSep) and separated on capillary columns (30 cm × 150 µm ID, PepSep) both packed with 1.9 µmC18 ReproSil and separated with a 30 min linear gradient from 3 to 30% acetonitrile and 0.1% formic acid and a flow rate of 500 nl min^{-1}. Both mass spectrometry (MS) and tandem MS (MS/MS) scans were acquired in the Orbitrap analyser with a resolution of 60,000 for MS scans and 30,000 for MS/MS scans. Higher-energy collisional dissociation fragmentation with 35% normalized collision energy was applied. A top-speed data-dependent MS/MS method with a fixed cycle time of 3 s was used. Dynamic exclusion was applied with a repeat count of 1 and an exclusion duration of 30 s; singly charged precursors were excluded from selection. Minimum signal threshold for precursor selection was set to 50,000. Predictive automatic gain control was used with a target value of 4×10^5 for MS scans and 5×10^4 for MS/MS scans. EASY-IC was used for internal calibration. Raw MS data files were analysed with MaxQuant v.1.6.2.2 (ref. 48). Database search was performed with Andromeda integrated in MaxQuant. The search was performed against the *E. coli* K-12 database appended with the Bil system proteome as well as common laboratory contaminants. The search was performed with tryptic cleavage specificity with three allowed miscleavages. Protein identification was under control of the false-discovery rate (FDR less than 1% FDR on protein and peptide spectrum match level). In addition to MaxQuant default settings, the search was performed against the following variable modifications: protein N-terminal acetylation, Gln to pyro-Glu formation (N-term. Gln) and oxidation (Met).

Negative staining electron microscopy

For negative staining, formvar and carbon-coated nickel grids (300 mesh, Electron Microscopy Sciences) were glow discharged in an Evactron CombiClean Decontaminator (XEI Scientific) for 1 min at 0.53 mbar (air) and 18 W. Next, 3 µl of phage sample was directly applied to the grid, incubated for 1 min and then blotted with filter paper (Whatman Grade 1). The grid was briefly washed on a drop of water and blotted with filter paper. Staining was performed by touching a 15 µl drop of staining solution (freshly made 2% ammonium molybdate, pH 6.5), followed by blotting with filter paper. This step was repeated once and then the grid was floated on top of a 15 µl drop of staining solution for 1 min. Finally, the grid was blotted with filter paper and air dried. Imaging was performed using a Tecnai T12 transmission electron microscope (Thermo Fisher Scientific) at an accelerating voltage of 120 kV, with a TVIPS TemCam-XF416 CMOS camera and SerialEM acquisition software[49].

Immunogold labelling electron microscopy

For immunogold labelling, a previously published protocol was followed with some changes[50]. Formvar and carbon-coated nickel grids (300 mesh) were glow discharged as above. Next, 3 µl of phage sample was directly applied to the grid, incubated for 1 min and then blotted with filter paper. The grid was briefly washed on a drop of water, blotted with filter paper and floated on a 20 µl drop of blocking buffer (PBS with 0.1% Tween 20 and 0.3% IgG-free BSA) for 30 min in a closed, humidified chamber. The grid was blotted with filter paper and floated on a 20 µl drop of primary anti-HA antibody (Sigma Aldrich, catalogue no. H6908) diluted 1:500 in blocking buffer for 1 h in a closed, humidified chamber. Following blotting with filter paper, the grid was washed five times by floating it on a 20 µl drop of wash buffer (PBS with 0.1% Tween 20 and 0.03% IgG-free BSA) for 3 min and blotted with filter paper after each wash. Next, the grid was floated on a 20 µl drop of anti-rabbit secondary antibody coupled to 6 nm colloidal gold particles (Electron Microscopy Sciences, catalogue no. 25104) diluted 1:50 in blocking buffer for 1 h in a closed, humidified chamber. The grid was washed as before, briefly washed twice on drops of water, blotted with filter paper and stained as described above. Imaging was performed as described above.

NTA

For NTA, phages were purified as described above, except that the final concentration step after dialysis was skipped and the volumes of the phage samples was increased to 1.25 ml by addition of buffer (20 mM Tris-HCl, pH 7.5, 150 mM NaCl, 10 mM $MgSO_4$). Next, 1 ml of each

phage sample (negative control, diluted 1:100; Bil system, low-density band, diluted 1:10; Bil system, high-density band, undiluted; mutant Bil system, diluted 1:100) was injected into the flow cell of a NanoSight NS300 instrument (Malvern Panalytical) equipped with a 405 nm laser. Measurements were performed using the NanoSight NTA v.3.4 software with the following parameters: the camera level was set to 10 and for each sample a standard measurement with three captures of 60 s per sample was run. The captured data were analysed and exported using the default parameters of the standard measurement protocol with a detection threshold of 2. To obtain the final numbers of phage particles per ml, the reported values were multiplied with the respective dilution factors of each sample. The same phage samples were used to measure PFUs using plaque assays as described above, except that a wild-type *E. coli* strain without plasmids was used as the indicator strain and no arabinose was added to the medium.

Adsorption and DNA injection assays

Phage adsorption rates were measured as described before[51], with some changes. To measure the relative amount of adsorbed phages propagated on wild-type and mutant Bil systems, 50 ml of wild-type *E. coli* was grown to an OD_{600} of 0.3 and then infected with purified phages at an MOI of 1. To ensure addition of the same amount of phage particles between conditions, MOI calculations were based on NTA measurements. Immediately after addition of the phages, 5 ml of culture was sampled and washed three times with ice-cold TBS to remove free phages from the bacteria. This corresponds to $t = 0$ min. Another 5 ml of culture was sampled each 5 and 10 min after infection and washed as before. After the three washes, DNA was extracted from the bacterial pellets using the DNeasy Blood and Tissue kit (Qiagen) according to the manufacturer's instructions.

To quantify the relative intracellular phage DNA concentrations, 25 ng of isolated DNA per sample was subjected to quantitative PCR (qPCR) using two primer pairs each (Supplementary Table 7) to measure amounts of phage (JHO-0283/0284 and JHO-0285/286) and bacterial (JHO-0289/0290 and JHO-0293/0294) DNA using Takyon No ROX SYBR 2X MasterMix blue dTTP qPCR kit (Eurogentech). For each sample, the average cycle threshold quantification (C_q) value of the two primer pairs for the phage and bacterial DNA was calculated and linearized by calculating $2^{(-Cq)}$. The linearized phage C_q values were then divided by the corresponding linearized bacterial C_q values to obtain the relative amount of phage DNA versus bacterial DNA. Finally, the ratio of phage to bacterial DNA was normalized by dividing it by the ratio at $t = 0$.

Efficiency of centre of infection assays

To measure the efficiency of centre of infection for phages propagated on wild-type and mutant Bil systems, 1 ml of wild-type *E. coli* was grown to an OD_{600} of 0.3 and then infected with purified phages at an MOI of 1. To ensure addition of the same amount of phage particles between conditions, MOI calculations were based on NTA measurements. After 30 min of adsorption, the bacteria were washed three times with PBS to remove free phages and finally resuspended in 1 ml of PBS. The bacteria with pre-adsorbed phages were serially diluted and spotted on lawns of wild-type *E. coli* as described above. The next day, centres of infection were counted.

Structural predictions

Structural predictions of proteins and complexes was performed using AlphaFold2 (ref. 16) and AlphaFold-Multimer[19], respectively. The predictions were run through ColabFold v.1.5.2 (ref. 52) using default parameters. To compare the structures of proteins and domains and calculate the respective root mean square deviation (r.m.s.d.) values, the best-ranking structure predictions were chosen and aligned using the 'super' method in the alignment plugin of PyMOL v.2.5.5 (ref. 53). To visualize these aligned structures, they were exported from PyMOL in their aligned states and imported into UCSF ChimeraX v.1.6.1 (ref. 54), where the structure images were generated.

Sequence conservation analysis

To analyse conserved residues, 77 non-redundant BilA homologues collected in a previous study[13] were aligned using Clustal Omega[55] using default parameters. Sequence logos were generated using WebLogo (https://weblogo.berkeley.edu/logo.cgi). Of the aligned proteins[13] (Supplementary Table 6), 12 contained short (2–9 amino acids) overhangs downstream of the conserved C-terminal glycine, which are not shown in the sequence logo for clarity. A reduced multiple sequence alignment was visualized using ESPript[56].

To compare the proteomes of SECphi27 (National Center for Biotechnology Information (NCBI) taxonomy ID 2496550) and SECphi4 (NCBI taxonomy ID 2729542), an all-versus-all blast analysis was performed using blastp[57,58]. Alignments with a threshold of 1×10^{-5} were considered as hits.

RNA extraction and RNA-seq

For RNA extraction, *E. coli* expressing the Bil system under control of a tetracycline-inducible promoter was grown to mid-log phase with 25 ng ml^{-1} aTc as inducer. *Caulobacter* sp. Root343 was grown to mid-log, late-log or early stationary phase. For each sample, a culture volume corresponding to an OD_{600} of 2 was taken and immediately mixed with a one-quarter volume of stop mix (95% ethanol, 5% saturated phenol) and frozen in liquid nitrogen. The samples were then thawed on ice followed by centrifugation at 4,000*g* and 4 °C for 10 min. The supernatant was discarded and the cell pellets resuspended in 1 ml of TRIzol (Thermo Scientific) followed by RNA extraction according to the manufacturer's protocol. The resulting RNA pellet was dissolved in 40 µl of water. To get rid of contaminating DNA, 0.5 µl of water, 5 µl DNase I buffer with $MgCl_2$ (Thermo Scientific), 0.5 µl of RNase inhibitor (Thermo Scientific) and 4 µl DNase I (Thermo Scientific) were added and the mixture incubated at 37 °C for 30 min. The DNase-digested RNA was subjected to acidic phenol-chloroform extraction and finally dissolved in 30 µl of water.

For library construction, the RNA was depleted of ribosomal RNA using a commercial ribosomal RNA depletion kit for mixed bacterial samples (Lexogen, RiboCop META, catalogue no. 125) and fragmented using ultrasound (two pulses of 30 s at 4 °C). Then, an oligonucleotide adaptor was ligated to the 3′ end of the RNA molecules. First-strand complementary DNA (cDNA) synthesis was performed using M-MLV reverse transcriptase with the 3′ adaptor as primer. After purification, the 5′ Illumina TruSeq sequencing adaptor was ligated to the 3′ end of the antisense cDNA. The resulting cDNA was PCR-amplified using a high-fidelity DNA polymerase and the barcoded TruSeq-libraries were pooled in roughly equimolar amounts. Sequencing of pooled libraries, spiked with PhiX control library, was performed at roughly 10 million reads per sample in single-ended mode with 100 cycles on the NextSeq 2000 platform (Illumina). Demultiplexed FASTQ files were generated with bcl-convert v.4.2.4 (Illumina).

RNA-seq data analysis

Raw reads were quality and adaptor trimmed using Trim Galore v.0.6.7 (https://github.com/FelixKrueger/TrimGalore) with default parameters. Trimmed reads were then mapped to the *E. coli* MG1655 (NC_000913.3) or *Caulobacter* sp. Root343 (GCF_001425745.1) genomes using BBMap v.39.06 (https://sourceforge.net/projects/bbmap/) with default parameters. Aligned reads were then assigned genes and quantified using featureCounts v.2.0.3 (ref. 59) with -s 1. Defence systems were predicted using DefenseFinder[60] and manually integrated into the reference annotations. The resulting quantified reads were normalized as transcripts per kilobase million and filtered by removing genes with fewer than ten average raw read counts over all three replicates. Then, the transcripts per kilobase million values were $\log_2$

transformed, sorted by these $\log_2$ values and the average of each gene plotted (Extended Data Fig. 2b,c).

Reporting summary

Further information on research design is available in the Nature Portfolio Reporting Summary linked to this article.

Data availability

The mass spectrometry proteomics data have been deposited to the ProteomeXchange Consortium by means of the PRIDE partner repository[61] with the dataset identifier PXD044622. The RNA-seq data have been deposited in NCBI's Gene Expression Omnibus[62] and are accessible through Gene Expression Omnibus series accession number GSE262579. Plasmid inserts of the constructs used are available in Supplementary Table 5. Uncropped images of gels and blots from all figures are presented in Supplementary Fig. 1. Source data are provided with this paper.

44. Chen, I. A. et al. The IMG/M data management and analysis system v.7: content updates and new features. *Nucleic Acids Res.* **51**, D723–d732 (2023).
45. Chung, C. T. & Miller, R. H. Preparation and storage of competent *Escherichia coli* cells. *Methods Enzymol.* **218**, 621–627 (1993).
46. Mazzocco, A., Waddell, T. E., Lingohr, E. & Johnson, R. P. Enumeration of bacteriophages using the small drop plaque assay system. *Methods Mol. Biol.* **501**, 81–85 (2009).
47. Schneider, C. A., Rasband, W. S. & Eliceiri, K. W. NIH Image to ImageJ: 25 years of image analysis. *Nat. Methods* **9**, 671–675 (2012).
48. Cox, J. & Mann, M. MaxQuant enables high peptide identification rates, individualized p.p.b.-range mass accuracies and proteome-wide protein quantification. *Nat. Biotechnol.* **26**, 1367–1372 (2008).
49. Mastronarde, D. N. Automated electron microscope tomography using robust prediction of specimen movements. *J. Struct. Biol.* **152**, 36–51 (2005).
50. Gulati, N. M., Torian, U., Gallagher, J. R. & Harris, A. K. Immunoelectron microscopy of viral antigens. *Curr. Protoc. Microbiol.* **53**, e86 (2019).
51. Ofir, G. et al. DISARM is a widespread bacterial defence system with broad anti-phage activities. *Nat. Microbiol.* **3**, 90–98 (2018).
52. Mirdita, M. et al. ColabFold: making protein folding accessible to all. *Nat. Methods* **19**, 679–682 (2022).
53. The PyMOL Molecular Graphics System v.1.8 (Schrödinger LLC, 2015).
54. Pettersen, E. F. et al. UCSF ChimeraX: structure visualization for researchers, educators, and developers. *Protein Sci.* **30**, 70–82 (2021).
55. Sievers, F. et al. Fast, scalable generation of high-quality protein multiple sequence alignments using Clustal Omega. *Mol. Syst. Biol.* **7**, 539 (2011).
56. Robert, X. & Gouet, P. Deciphering key features in protein structures with the new ENDscript server. *Nucleic Acids Res.* **42**, W320–W324 (2014).
57. Altschul, S. F. et al. Gapped BLAST and PSI-BLAST: a new generation of protein database search programs. *Nucleic Acids Res.* **25**, 3389–3402 (1997).
58. Altschul, S. F. et al. Protein database searches using compositionally adjusted substitution matrices. *FEBS J.* **272**, 5101–5109 (2005).
59. Liao, Y., Smyth, G. K. & Shi, W. featureCounts: an efficient general purpose program for assigning sequence reads to genomic features. *Bioinformatics* **30**, 923–930 (2014).
60. Tesson, F. et al. Systematic and quantitative view of the antiviral arsenal of prokaryotes. *Nat. Commun.* **13**, 2561 (2022).
61. Perez-Riverol, Y. et al. The PRIDE database resources in 2022: a hub for mass spectrometry-based proteomics evidences. *Nucleic Acids Res.* **50**, D543–d552 (2022).
62. Edgar, R., Domrachev, M. & Lash, A. E. Gene Expression Omnibus: NCBI gene expression and hybridization array data repository. *Nucleic Acids Res.* **30**, 207–210 (2002).
63. Kanamaru, S. et al. Structure of the cell-puncturing device of bacteriophage T4. *Nature* **415**, 553–557 (2002).

Acknowledgements We thank the Sorek laboratory members for comments on earlier versions of this paper. We thank A. Savidor and M. Kupervaser at the De Botton Protein Profiling Institute at the Weizmann Institute as well as S. Lamer at the Rudolf Virchow Center for help with mass spectrometry data generation and analysis. We thank the Core Unit SysMed at the University of Würzburg for technical support by E. Katzowitzsch and RNA-seq data generation. This work was supported in part by the Interdisciplinary Center for Clinical Research (IZKF) Würzburg (project no. Z-6). We also thank J. Vogel and the Helmholtz Institute for RNA-based Infection Research for help in difficult times. J.H. was funded by the Deutsche Forschungsgemeinschaft (DFG, German Research Foundation), grant no. 466645764 and a fellowship from the Council for Higher Education and Israel Academy of Science and Humanities (CHE/IASH) Excellence Fellowship Program for International Postdoctoral Researchers. R.S. was supported, in part, by the European Research Council (grant no. ERC-AdG GA 101018520), Israel Science Foundation (MAPATS grant no. 2720/22), the Deutsche Forschungsgemeinschaft (SPP 2330, grant no. 464312965), the Ernest and Bonnie Beutler Research Program of Excellence in Genomic Medicine, the Dr. Barry Sherman Institute for Medicinal Chemistry, M. de Botton, the Andre Deloro Prize and the Knell Family Center for Microbiology.

Author contributions J.H. and R.S. conceived and designed the study. J.H. performed the experiments. S.G.W. performed electron microscopy. J.H. and R.S. analysed the data. J.H. visualized the data. R.S. acquired funding. J.H. and R.S. wrote the original draft of the manuscript. All authors reviewed and edited the manuscript and support the conclusions.

Competing interests R.S. is a scientific cofounder and adviser of BiomX and Ecophage. The remaining authors declare no competing interests.

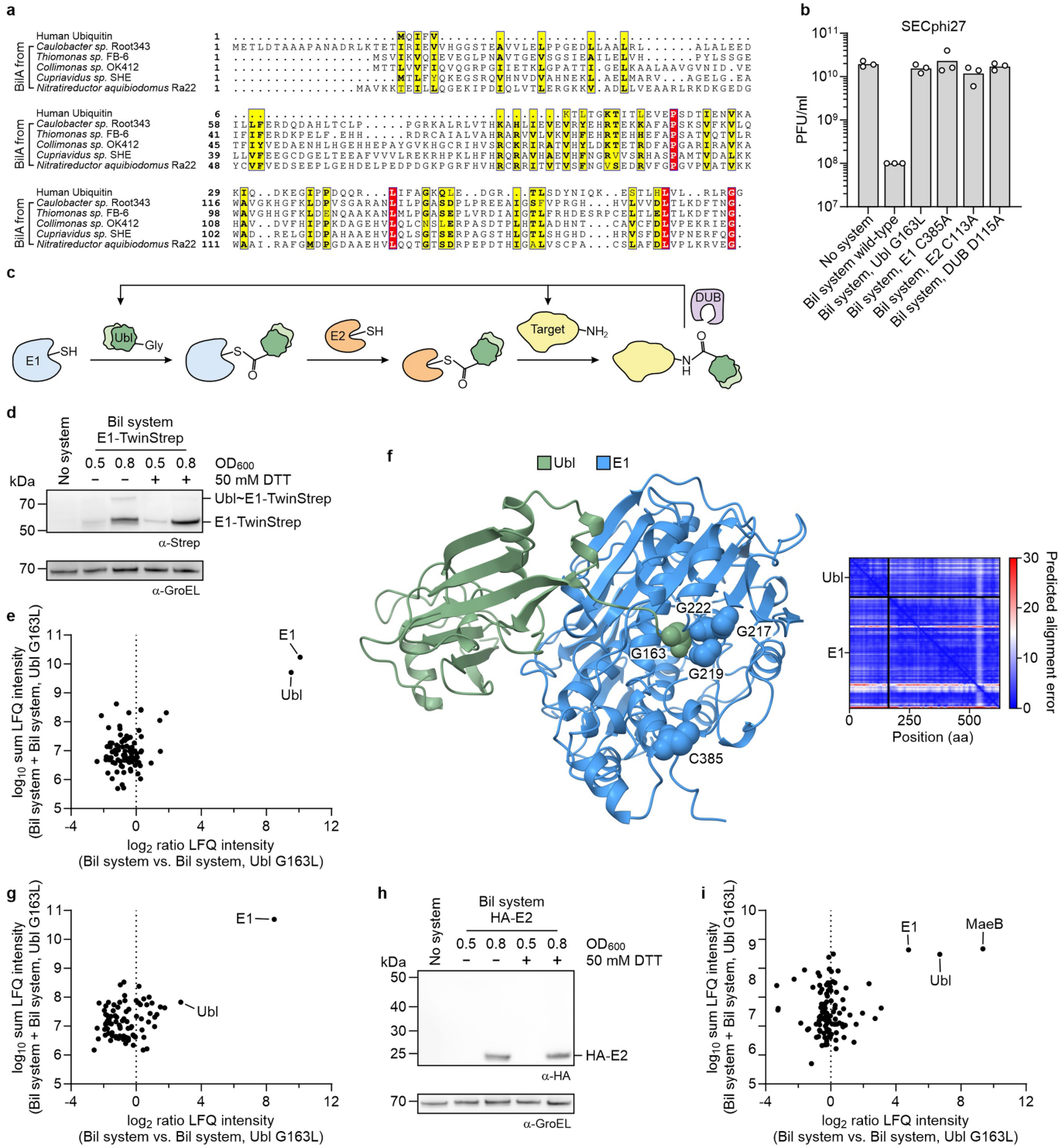
Additional information

Supplementary information The online version contains supplementary material available at https://doi.org/10.1038/s41586-024-07616-5.

Correspondence and requests for materials should be addressed to Rotem Sorek.

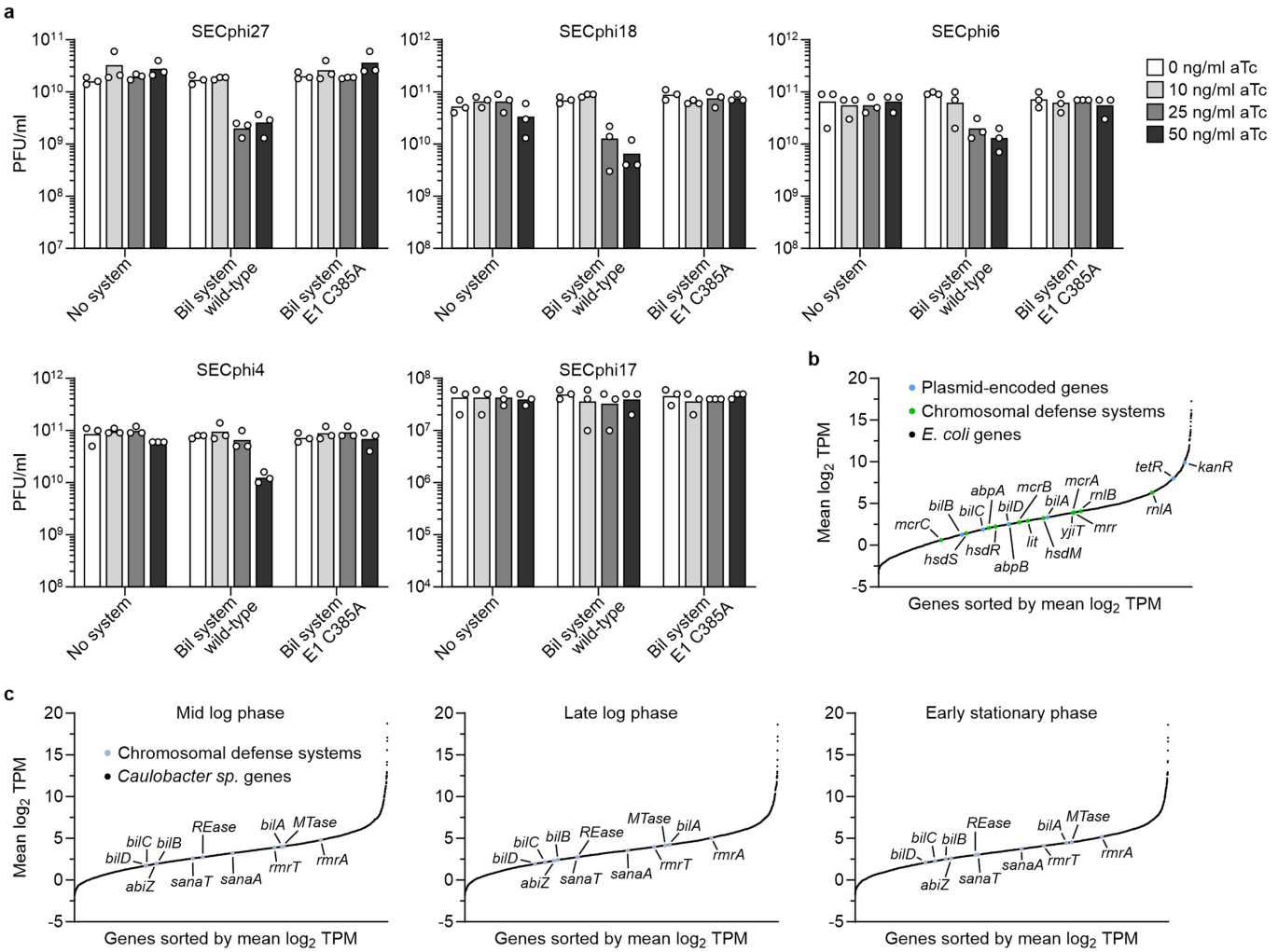
Peer review information *Nature* thanks Edze Westra and the other, anonymous, reviewer(s) for their contribution to the peer review of this work.

Reprints and permissions information is available at http://www.nature.com/reprints.

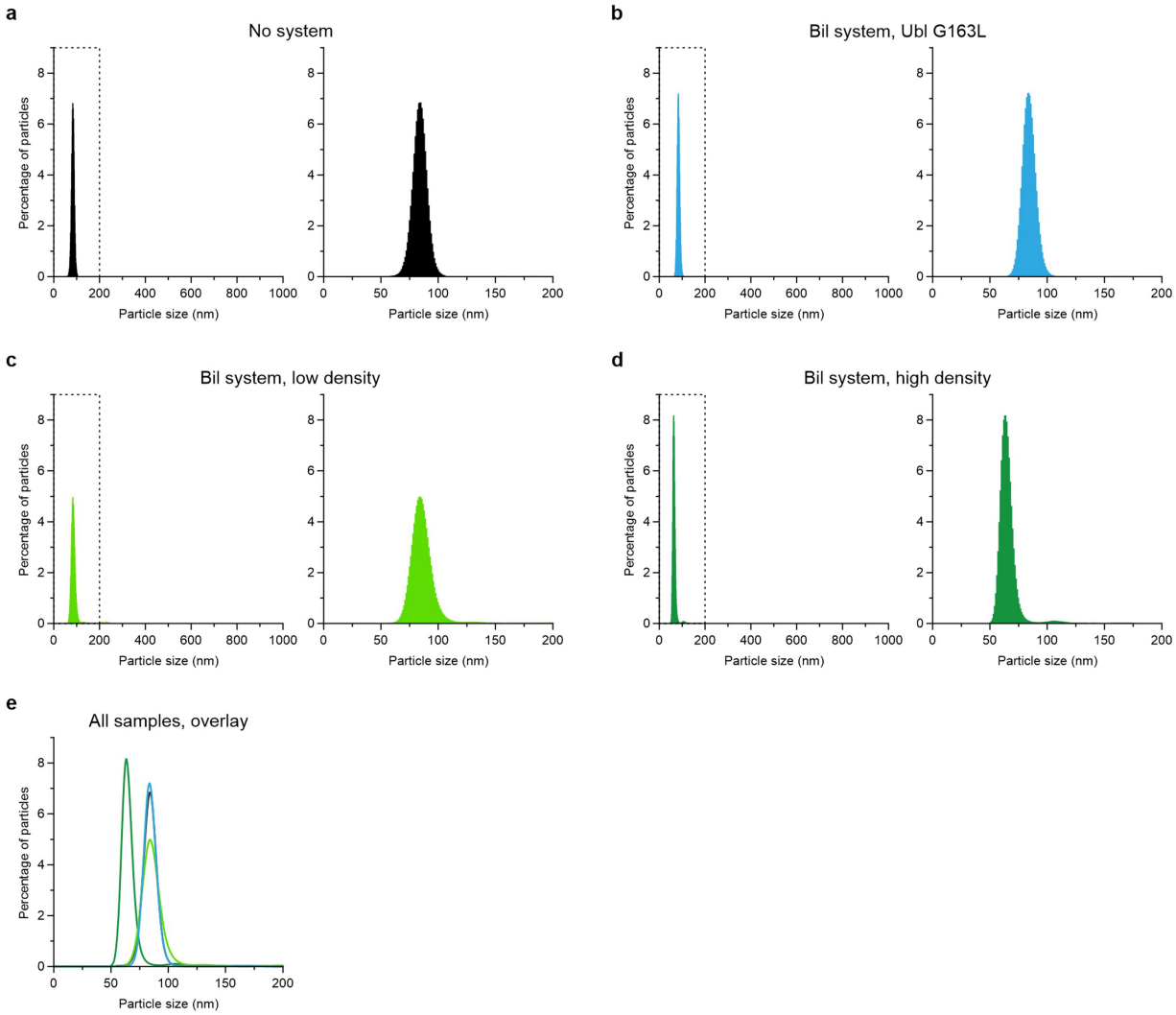


Extended Data Fig. 1 | See next page for caption.

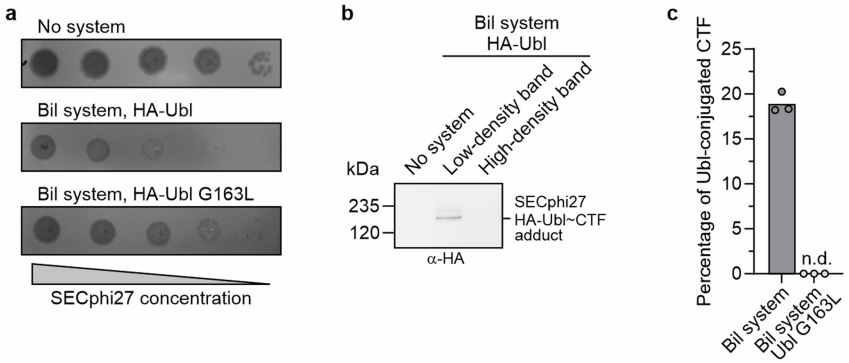
Extended Data Fig. 1 | Interactions between the Bil Ubl and the E1/E2 enzymes. a, Multiple sequence alignment of human Ubiquitin and five BilA Ubl homologs. Residues highlighted in bold and yellow have a global similarity score of ≥ 0.7. Residues highlighted in bold and red are fully conserved. Visualized using ESPript[56]. Related to Fig. 1c. **b**, PFU quantification of plaque assays shown in Fig. 1d. Data, except for the Ubl G163L mutant, were taken from[13]. Bars represent the average of three biological replicates with individual data points overlaid. **c**, Enzymatic reaction in Ubl-conjugating pathways. The active site cysteine of the E1 protein forms a thioester with the C-terminal glycine of the Ubl, which is then transferred to the active site cysteine of the E2 to form another thioester. The E2 then transfers the Ubl to a lysine residue of the target protein. Deubiquitinases (DUBs) can reverse the conjugation by cleaving the Ubl off the target protein. **d**, Western blot of whole cell lysates of bacteria expressing the Bil system with a tagged E1. Two bands for the E1 are revealed. The upper band of ~70 kDa band is reduced by DTT, indicating a thioester bond between the E1 and the Ubl. GroEL was used as loading control on the same blot. Cells at OD_{600} of 0.8 are infected by phage SECphi27. A representative image of two biological replicates is shown. **e**, Mass spectrometry analysis of the ~70 kDa band observed in Ubl immunoprecipitation experiments verifies that it included the Ubl-E1 complex (related to Fig. 1e). The $\log_{10}$ of the sum of the label-free quantification (LFQ) intensity values obtained from wild-type and mutant Bil system for each detected protein was plotted against the $\log_2$ ratio of the LFQ intensities of the Bil system vs. the mutant Bil system. **f**, AlphaFold-Multimer[19] prediction of the interaction between the Ubl and the E1. A high confidence structure (model confidence of 0.94 and overall low predicted alignment error, right side of the panel) shows G163 (indicated as spheres) of the Ubl to be positioned at the nucleotide-binding loop of the E1 (G217, G219 and G222; indicated as spheres). **g**, Mass spectrometry analysis of the ~50 kDa band observed in Ubl immunoprecipitation experiments verifies the E1 protein (related to Fig. 1e). Data analyzed and plotted as in **e**. **h**, Western blot of whole cell lysates of bacteria expressing the Bil system with a tagged E2. No covalent complex of the E2 could be observed. GroEL was used as loading control on the same blot. Cells at OD_{600} of 0.8 are infected by phage SECphi27. A representative image of three biological replicates is shown. **i**, Mass spectrometry analysis of the ~80 kDa band observed in Ubl immunoprecipitation experiments (related to Fig. 1e). Data analyzed and plotted as in **e**. MaeB is identified in this band, but as the molecular weight of MaeB is 82 kDa, it is likely pulled down unspecifically and not conjugated to the Ubl.



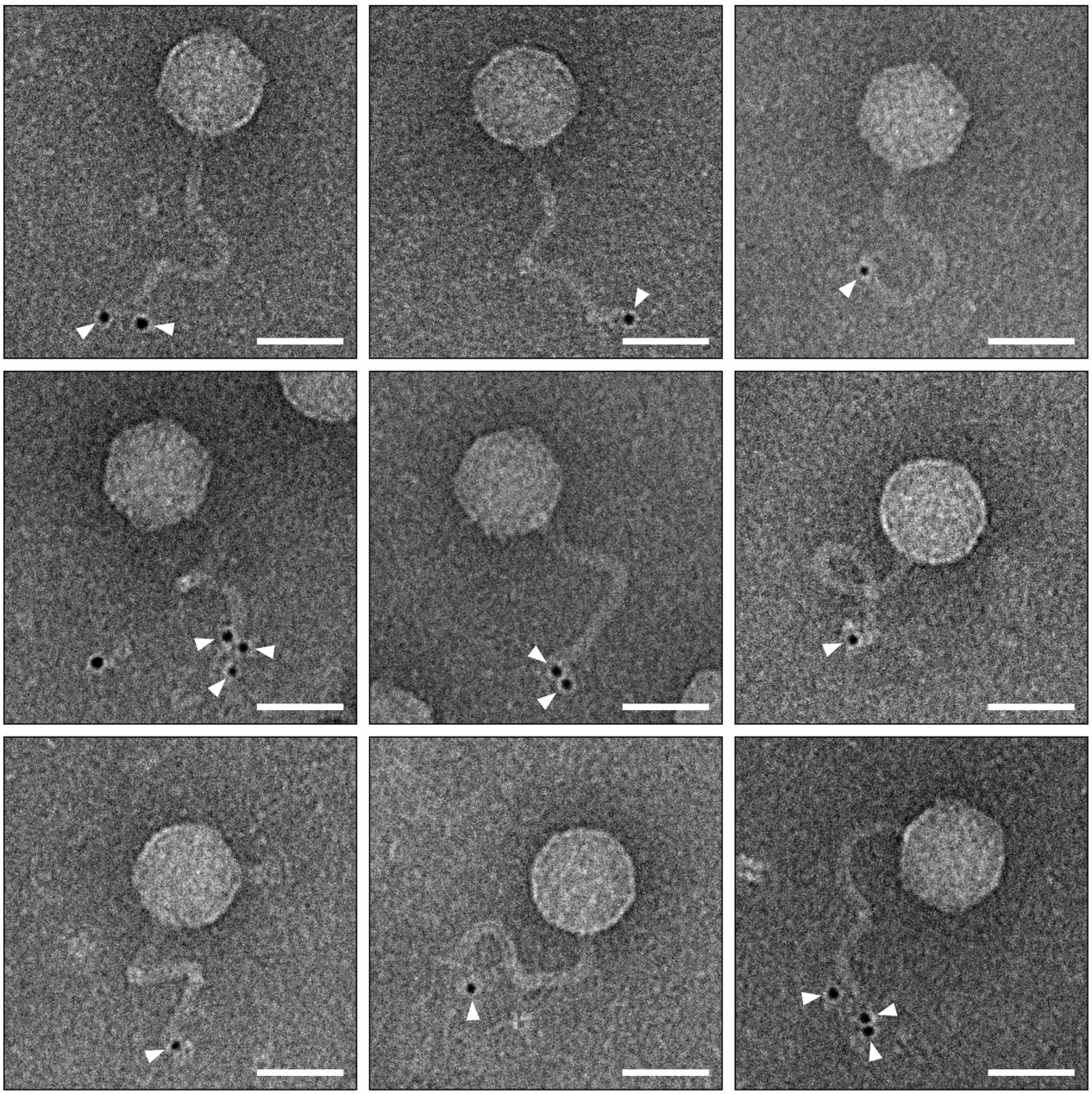
Extended Data Fig. 2 | The Bil system provides defense at expression levels relevant to physiological conditions. a, PFU quantification of different phages infecting *E. coli* expressing the Bil system from a plasmid with a p15A origin (estimated ~10 copies per cell) under the control of a tetracycline-inducible promoter. Four different concentrations of inducer (anhydrotetracycline, aTc) were used. Bars represent the average of three biological replicates with individual data points overlaid. **b**, RNA-sequencing data of Bil-expressing *E. coli* with expression induced using 25 ng/ml of aTc (see **a**). Data show average $\log_2$ transcripts per kilobase million (TPM) of each gene with ≥ 10 average raw reads in three biological replicates, sorted by their $\log_2$ TPM values. Blue, plasmid-encoded Bil system transcripts (*bilA*, *bilB*, *bilC*, *bilD*), tetracycline repressor (*tetR*) and aminoglycoside phosphotransferase (*kanR*). Green, chromosomally encoded defense systems of *E. coli* MG1655, predicted using DefenseFinder[60]: RM type I (*hsdM*, *hsdR*, *hsdS*), RM type IV (*mcrA*, *mcrB*, *mcrC*, *mrr*), Lit (*lit*), RnlAB (*rnlA*, *rnlB*), Hachiman (*abpA*, *abpB*) and Druantia type III (*yjiT*). CRISPR genes are not shown for clarity. **c**, RNA-sequencing data of *Caulobacter sp.* Root343 at the indicated growth phases. Data show average $\log_2$ transcripts per kilobase million (TPM) of each gene with ≥ 10 average raw reads in three biological replicates, sorted by their $\log_2$ TPM values. Light blue, chromosomally encoded defense systems of *Caulobacter sp.* Root343, predicted using DefenseFinder[60]: Bil system (*bilA*, *bilB*, *bilC*, *bilD*), RM type II (*MTase*, *REase*), SanaTA (*sanaA*, *sanaT*), RosmerTA (*rmrA*, *rmrT*) and AbiZ (*abiZ*).



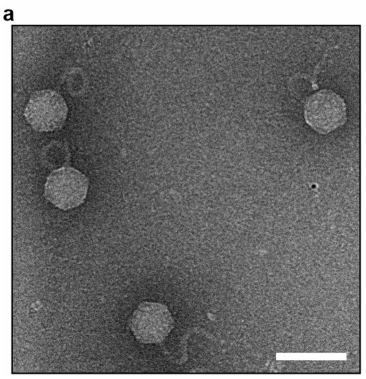
Extended Data Fig. 3 | Phage particle size measurements. a-d, Particle size distributions of phages isolated from bacteria expressing the indicated systems, measured by nanoparticle tracking analysis. Bars represent the average of three biological replicates. The dashed areas of each graph are magnified on the right of each graph. High and low density indicate phages isolated from high- and low-density bands in the CsCl gradient. **e**, Overlay of the particle size distributions shown in **a-d**.

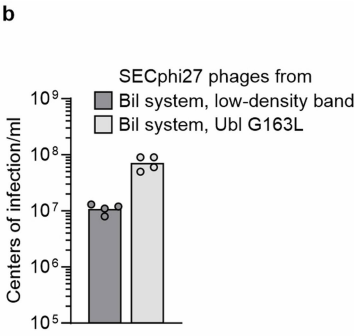


Extended Data Fig. 4 | The phage central tail fibre is the target of the Bil system. a, Plaque assays showing that addition of an HA-tag to the Ubl of the Bil system does not interfere with phage defense. **b**, Immunoprecipitation of HA-tagged Ubl protein from SECphi27 isolated from bacteria expressing the Bil system, analyzed by western blotting. Phages from the low- and high-density bands of the CsCl gradient were immunoprecipitated separately. A representative image of two biological replicates is shown. **c**, Quantification of the percentage of Ubl-conjugated CTF from the total amount of CTF detected by western blotting (related to Fig. 3c). n.d., not detected. Bars represent the average of three biological replicates with individual data points overlaid.

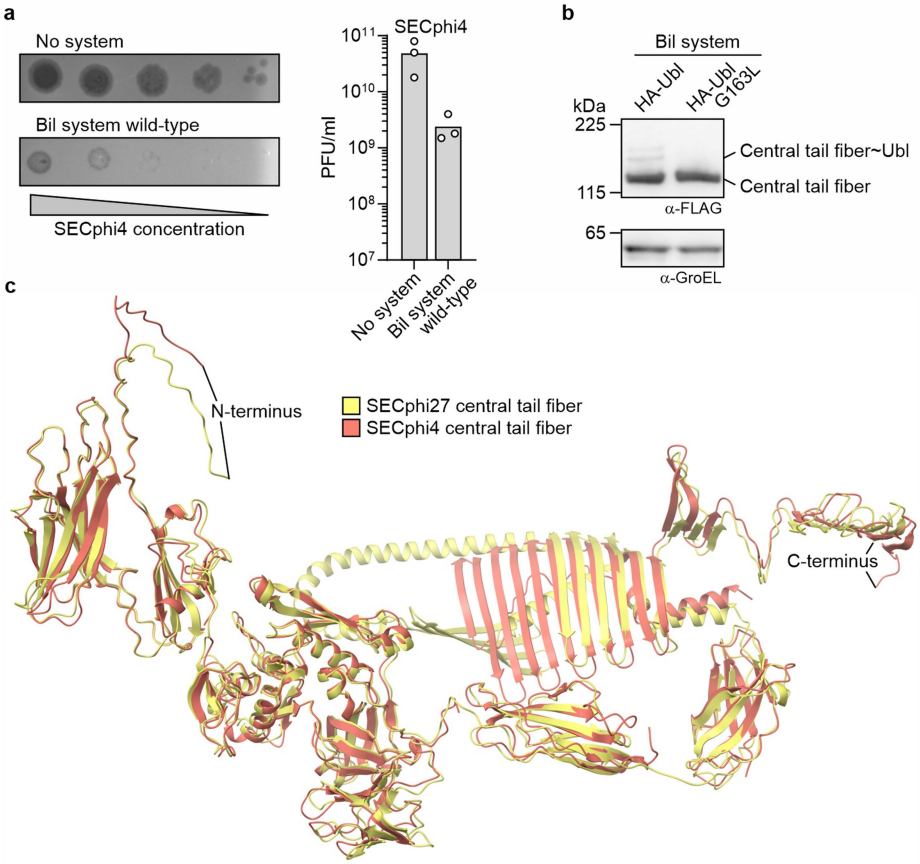


Extended Data Fig. 5 | The Bil system modifies the tip of the phage tail. Immunogold labeling transmission electron microscopy images of SECphi27 phages isolated from bacteria expressing the HA-Ubl Bil system (related to Fig. 3d). White arrowheads represent gold labeling of HA-Ubl. Scale bars represent 50 nm.

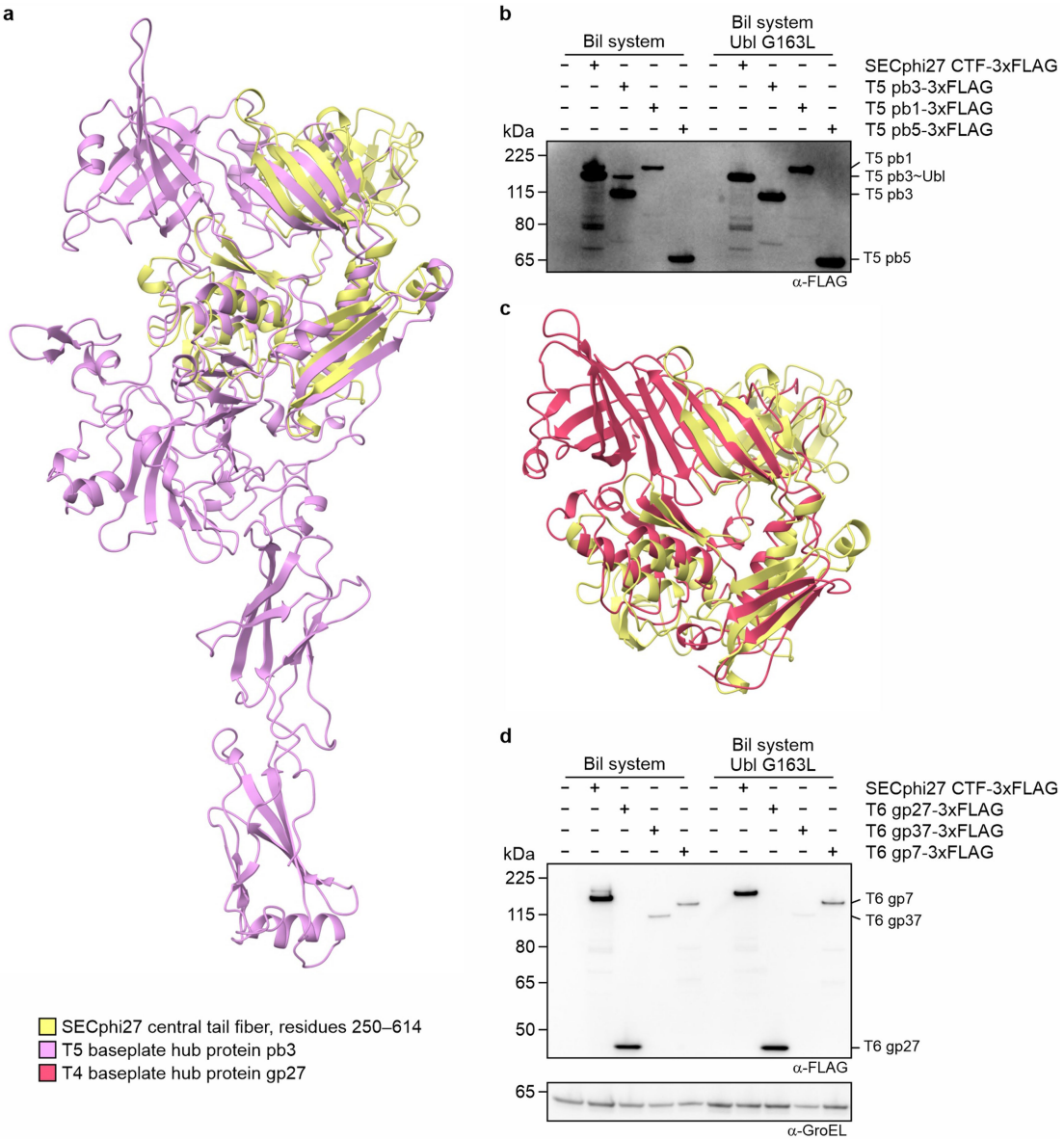




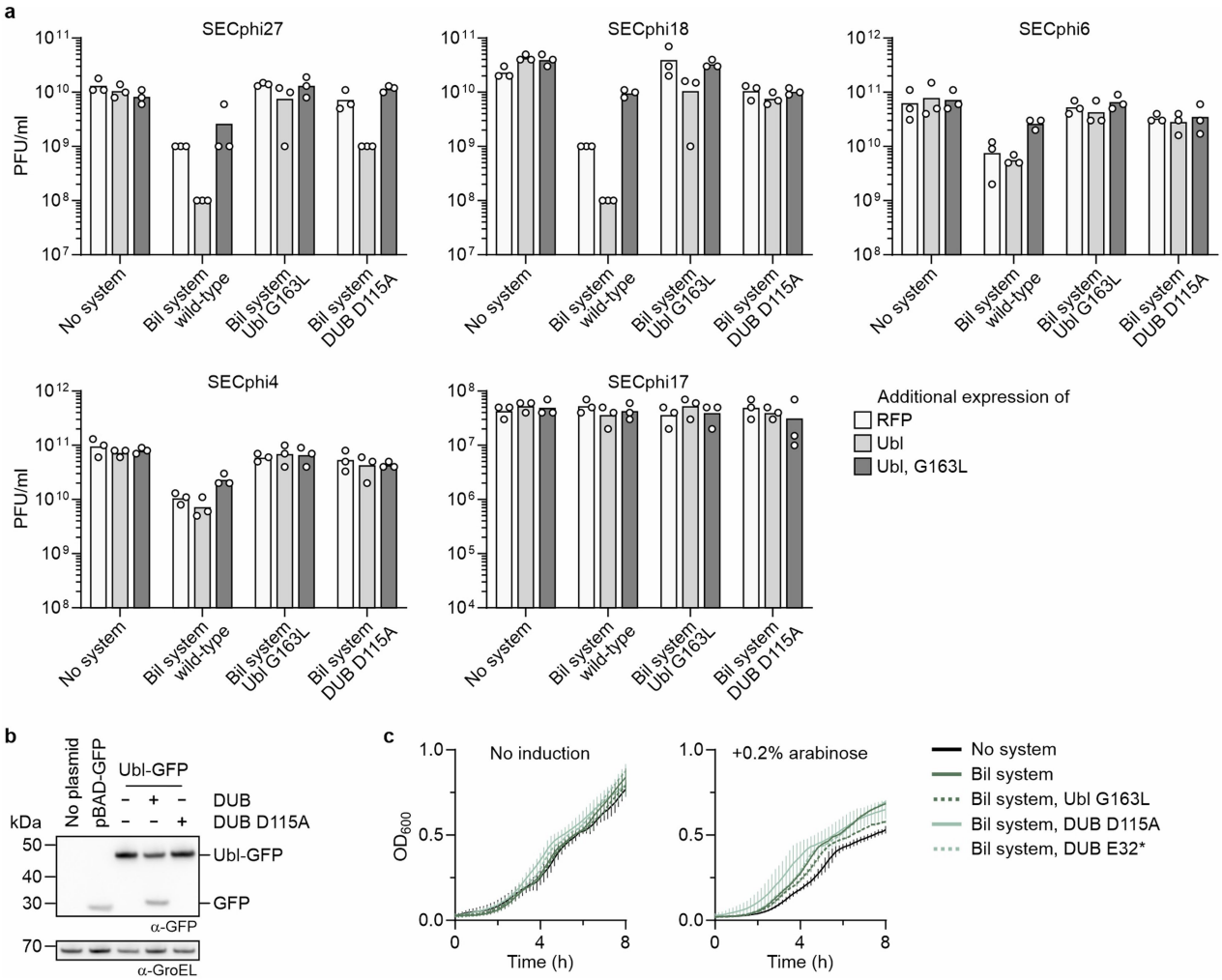
Extended Data Fig. 6 | The central tail fiber is a conserved structure targeted by the Bil system. a, Representative immunogold labeling transmission electron microscopy image of SECphi27 phages isolated from bacteria expressing mutant HA-Ubl Bil system. No gold labeling could be observed on the phages. Scale bar represents 100 nm. **b**, Efficiency of center of infection assays with phages propagated on either the wild-type or the mutant Bil systems. Wild-type *E. coli* cells were infected at MOI = 1 (numbers of phage particles were determined by NTA) and allowed to adsorb for 30 min. After washing, the bacteria with adsorbed phages were serially diluted and dropped on a lawn of wild-type *E. coli*. Centers of infection were counted the next day. Bars represent the average of four biological replicates with individual data points overlaid.



Extended Data Fig. 7 | The central tail fiber is a conserved structure targeted by the Bil system. a, Plaque assays showing the defense phenotype of the Bil systems against SECphi4. Data are representative of three biological replicates with quantification of the three replicates shown on the right (quantification data were taken from[13]). **b**, Co-expression of the Bil system with the central tail fiber of SECphi4, analyzed by western blotting. GroEL was used as loading control on the same blot. A representative image of two biological replicates is shown. **c**, AlphaFold2[16] predictions of the structures of the central tail fibers of SECphi27 (NCBI ID: YP_009965952.1) and SECphi4 (NCBI ID: QJI52569.1). The predicted structure of the SECphi4 central tail fiber was superimposed on the SECphi27 central tail fiber using the following domains: Residues 1–251 (RMSD = 0.91 Å), residues 252–628 (RMSD = 1.30 Å), residues 629–736 (RMSD = 1.11 Å), residues 737–829 (RMSD = 1.10 Å), residues 830–1139 (RMSD = 2.69 Å).



Extended Data Fig. 8 | Tail structure proteins of different phages contain structurally similar domains. a, AlphaFold2[16] prediction of residues 250–614 of the SECphi27 central tail fiber (related to Extended Data Fig. 7c) superimposed on the cryo-EM structure of T5 pb3 (PDB: 7ZQB[31]; RMSD = 2.01 Å). **b**, High exposure version of the western blot shown in Fig. 4c. **c**, AlphaFold2[16] prediction of residues 250–614 of the SECphi27 central tail fiber (related to Extended Data Fig. 7c) superimposed on the crystal structure of T4 gp27 (PDB: 1K28[63]; RMSD = 3.64 Å). **d**, Co-expression of the Bil system with either the central tail fiber (CTF) of SECphi27, the baseplate hub protein gp27 of T6, the large distal tail fiber subunit protein gp37 of T6 or the baseplate wedge subunit gp7 of T6, analyzed by western blotting. GroEL was used as loading control on the same blot. A representative image of two biological replicates is shown.



Extended Data Fig. 9 | The DUB is essential for the function of the Bil system and is able to cleave a Ubl fusion protein. a, PFU quantification of different phages infecting *E. coli* cells that co-express Bil system variants and Ubl, mutated Ubl or RFP control. Bars represent the average of three biological replicates with individual data points overlaid. **b**, Western blot of whole cell lysates of bacteria co-expressing a Ubl-GFP fusion protein and the DUB of the Bil system. GFP can be cleaved off the Ubl-GFP fusion protein by the DUB. GroEL was used as loading control on the same blot. A representative image of three biological replicates is shown. **c**, Growth curves of *E. coli* expressing Bil system variants either without (left) or with (right) the addition of expression inducer. The DUB E32* mutant is a single-nucleotide mutant replacing the amino acid at position 32 of the DUB protein with a stop codon. Data shown is the average of three biological replicates. Error bars show average with s.d.

nature portfolio

Corresponding author(s): Rotem Sorek

Last updated by author(s): May 8, 2024

Reporting Summary

Nature Portfolio wishes to improve the reproducibility of the work that we publish. This form provides structure for consistency and transparency in reporting. For further information on Nature Portfolio policies, see our Editorial Policies and the Editorial Policy Checklist.

Please do not complete any field with "not applicable" or n/a. Refer to the help text for what text to use if an item is not relevant to your study.
For final submission: please carefully check your responses for accuracy; you will not be able to make changes later.

Statistics

For all statistical analyses, confirm that the following items are present in the figure legend, table legend, main text, or Methods section.

n/a	Confirmed	
☐	☒	The exact sample size (*n*) for each experimental group/condition, given as a discrete number and unit of measurement
☐	☒	A statement on whether measurements were taken from distinct samples or whether the same sample was measured repeatedly
☒	☐	The statistical test(s) used AND whether they are one- or two-sided *Only common tests should be described solely by name; describe more complex techniques in the Methods section.*
☒	☐	A description of all covariates tested
☒	☐	A description of any assumptions or corrections, such as tests of normality and adjustment for multiple comparisons
☒	☐	A full description of the statistical parameters including central tendency (e.g. means) or other basic estimates (e.g. regression coefficient) AND variation (e.g. standard deviation) or associated estimates of uncertainty (e.g. confidence intervals)
☒	☐	For null hypothesis testing, the test statistic (e.g. *F*, *t*, *r*) with confidence intervals, effect sizes, degrees of freedom and *P* value noted *Give P values as exact values whenever suitable.*
☒	☐	For Bayesian analysis, information on the choice of priors and Markov chain Monte Carlo settings
☒	☐	For hierarchical and complex designs, identification of the appropriate level for tests and full reporting of outcomes
☒	☐	Estimates of effect sizes (e.g. Cohen's *d*, Pearson's *r*), indicating how they were calculated

Our web collection on statistics for biologists contains articles on many of the points above.

Software and code

Policy information about availability of computer code

Data collection	Nanoparticle tracking analysis data collection was performed using NanoSight NTA 3.4 software. Structure predictions were performed using ColabFold v1.5.2. Electron microscopy data collection was performed using SerialEM. Plate reader data was collected using Tecan iControl v3.8.2.0 software.
Data analysis	Nanoparticle tracking analysis data analysis was performed using NanoSight NTA 3.4 software. Structure analysis was performed using PyMOL 2.5.5. Mass spectrometry data was analyzed using PMI-Byonic-Com v4.6.1 or MaxQuant v1.6.2.2. RNA-seq data was analyzed using Trim Galore v0.6.7, BBMap v39.06 and featureCounts v2.0.3.

For manuscripts utilizing custom algorithms or software that are central to the research but not yet described in published literature, software must be made available to editors and reviewers. We strongly encourage code deposition in a community repository (e.g. GitHub). See the Nature Portfolio guidelines for submitting code & software for further information.

Data

Policy information about availability of data

All manuscripts must include a data availability statement. This statement should provide the following information, where applicable:

- Accession codes, unique identifiers, or web links for publicly available datasets
- A description of any restrictions on data availability
- For clinical datasets or third party data, please ensure that the statement adheres to our policy

Data that support the findings of this study are available within the article and its Supplementary Data. Gene accessions appear in the Methods section of the paper. Plasmid insert sequences of the constructs used for the experiments are attached as Supplementary Files. Additional data are available from the corresponding author upon request.

Research involving human participants, their data, or biological material

Policy information about studies with human participants or human data. See also policy information about sex, gender (identity/presentation), and sexual orientation and race, ethnicity and racism.

Reporting on sex and gender	NA
Reporting on race, ethnicity, or other socially relevant groupings	NA
Population characteristics	NA
Recruitment	NA
Ethics oversight	NA

Note that full information on the approval of the study protocol must also be provided in the manuscript.

Field-specific reporting

Please select the one below that is the best fit for your research. If you are not sure, read the appropriate sections before making your selection.

☒ Life sciences ☐ Behavioural & social sciences ☐ Ecological, evolutionary & environmental sciences

For a reference copy of the document with all sections, see nature.com/documents/nr-reporting-summary-flat.pdf

Life sciences study design

All studies must disclose on these points even when the disclosure is negative.

Sample size	Experiments were performed in triplicates unless otherwise stated without prior sample size calculation, as is standard for such experimental designs.
Data exclusions	No data was excluded.
Replication	Experiments were performed in triplicates unless otherwise stated, no failed replications occurred.
Randomization	No randomization was performed.
Blinding	No blinding was performed.

Reporting for specific materials, systems and methods

We require information from authors about some types of materials, experimental systems and methods used in many studies. Here, indicate whether each material, system or method listed is relevant to your study. If you are not sure if a list item applies to your research, read the appropriate section before selecting a response.

Materials & experimental systems

n/a	Involved in the study
☐	☒ Antibodies
☒	☐ Eukaryotic cell lines
☒	☐ Palaeontology and archaeology
☒	☐ Animals and other organisms
☒	☐ Clinical data
☒	☐ Dual use research of concern
☒	☐ Plants

Methods

n/a	Involved in the study
☒	☐ ChIP-seq
☒	☐ Flow cytometry
☒	☐ MRI-based neuroimaging

Antibodies

Antibodies used

The following antibodies were used:
rabbit anti-HA (Sigma Aldrich #H6908)
mouse anti-FLAG (Sigma Aldrich #F1804)
mouse anti-GFP (Sigma Aldrich #11814460001)
HRP-conjugated goat anti-rabbit secondary antibody (Thermo Scientific #31460)
HRP-conjugated goat anti-mouse secondary antibody (Thermo scientific #31430)
anti-GroEL antibody (Sigma Aldrich #G6532)

Validation

All antibodies used in this study are commercially available and their specificity was verified by both the manufacturers and many studies citing each of these antibodies.

This checklist template is licensed under a Creative Commons Attribution 4.0 International License, which permits use, sharing, adaptation, distribution and reproduction in any medium or format, as long as you give appropriate credit to the original author(s) and the source, provide a link to the Creative Commons license, and indicate if changes were made. The images or other third party material in this article are included in the article's Creative Commons license, unless indicated otherwise in a credit line to the material. If material is not included in the article's Creative Commons license and your intended use is not permitted by statutory regulation or exceeds the permitted use, you will need to obtain permission directly from the copyright holder. To view a copy of this license, visit http://creativecommons.org/licenses/by/4.0/